Concept development, floating bridge E39 Bjørnafjorden

Appendix E – Enclosure 7

10205546-08-NOT-098

Bridge closure due to wind

MEMO

PROJECT	Concept development, floating bridge E39 Bjørnafjorden	DOCUMENT CODE	10205546-08-NOT-098
CLIENT	Statens vegvesen	ACCESSIBILITY	Restricted
SUBJECT	Bridge closure due to wind	PROJECT MANAGER	Svein Erik Jakobsen
TO	Statens vegvesen	PREPARED BY	Ketil Aas-Jakobsen
COPY TO		RESPONSIBLE UNIT	AMC

SUMMARY

Bridge closure due to wind is discussed for the different bridge alignments in light of the turbulence data in the Metocean Design basis. The discussion shows that bridge closure due to wind may increase due to the increased turbulence intensity from the southern sector. We recommend that this is addressed by an updated analysis. To do these analysis sectorial long term distribution data of the wind is needed (e.g. Weibull parameters).

00	24.05.2019	Final issue	K. Aas-Jakobsen	R. M. Larssen	S. E. Jakobsen
REV.	DATE	DESCRIPTION	PREPARED BY	CHECKED BY	APPROVED BY

1 Bridge closure due to wind

The Metocean design basis provided in this project indicate that closure due to wind effects on vehicles should be re-evaluated. For certain wind direction the turbulence intensity is specified to 30% /2/ and this will reduce the wind speed for which closure of the bridge must be considered .

N400 states that the structure should be calculated with traffic load up to a 3s gust speed of 35 m/s (N400-§5.4.3.3 /4/). This can be understood as if the gust speed is above 35 m/s, no vehicles is on the bridge, i.e. the bridge is closed. The 3s gust speed can be approximated by $U_{3s} = U_{10min} + 3.5*\sigma_u$, where $\sigma_u = I_u * U_{10min}$. Thus, by increasing the turbulence intensity, U_{10min} is reduced.E.g. by setting U_{3s} to 35 m/s, the closure wind speed becomes:

A. I_u=11% => U_{10min} = 25.3 m/s
B. I_u=30% => U_{10min} = 17.1 m/s.

The criteria in A above give wind speed similar to closure wind speed used for other bridges worldwide, and similar to the criteria in the previous phase of the Bjørnafjorden crossing. As can be seen in B, if one applies the same method for 30% turbulence intensity, a significantly lower closure speed is found. A reduction of closure speed to this level will increase closure time significantly, and it is questionable if the up-time target for the bridge can be reached without taking measures.

The current Metocean design basis does not contain data about long term distribution, neither for sectorial or omnidirectional data, but by using the results from the calculations in the previous phase the following is found /5/:

- U_{10min} is above 25m/s 16 hours yearly
- U_{10min} is above 20m/s 69 hours yearly

Thus, a criteria of 17 m/s will give significantly more bridge closing due to wind than the current value of about 16 hours.

In this phase of the project the client has not asked specifically for up-time evaluation of the concepts, as it has not been deemed necessary. Calculations in previous phases has shown that the uptime fulfils the criteria of 99.5%, which corresponds to 43.8 hours of year closure /5/. The above calculation indicates that it will be challenging to reach the 99.5% target without detailed assessment.

In the previous analysis wind in the sector +/- 30 degrees to perpendicular to the vehicles has been viewed as particular important when assessing the effects, as the effective wind attack angle on the vehicle has a significant perpendicular component when one takes into account the speed of the vehicle itself. The critical direction compared to a linearized alignment segment is shown to the right in Figure 1.

Bridge closure due to wind

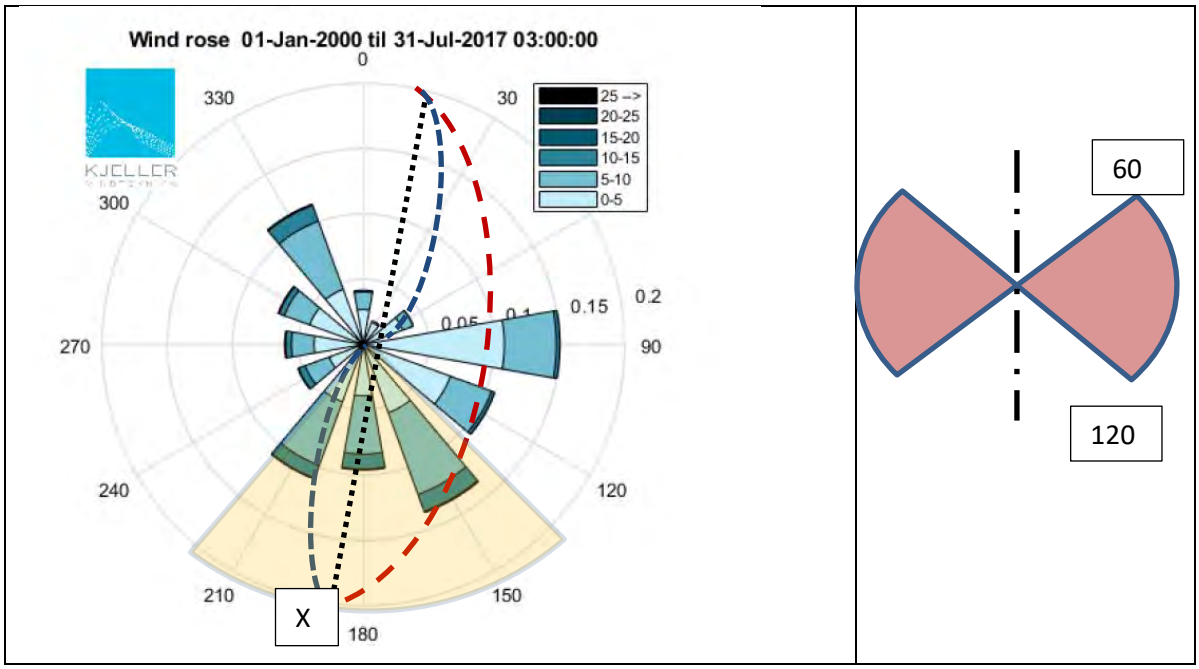

Figure 1 Left: Wind rose and area of increased turbulence intensity (Yellow), compared to K12 (Red), K13 (Black) and K14 (Blue).
Right: Critical wind direction compared to alignment (red).

The left part of Figure 1 shows the wind rose with superimposed alignments; K12 (red), K13 (black) and K14 (blue), and the wind direction zone for which elevated turbulence should be applied. Table 1 show a summary of these two figures combined. As can be seen from the table, closure time on Concept K12 and K13 may be affected by the elevated turbulence intensity from the southern sector.

Based on this evaluation we recommend that up-time is re-evaluated for the concepts based on the current Metocean Design Basis. For this sectorial long term distribution is needed, including Weibull parameters.

Table 1 Critical cross wind.

Concept	Alignment angle compared to North at point X in Figure 1 (approx.)	Wind gust direction relative to alignment	Within critical region marked red in Figure 1
K12	+ 35°	115° – 175°	Yes, partly. Detail assessment necessary
K13	+ 10°	200° – 140°	Close. Detail assessment necessary
K14	South: - 5° Mid point: +20°	155° – 215° (South) 130° – 190° (Mid point)	South: No Close. Detail assessment necessary

2 References

/1/ SBJ-32-C4-SVV-90-BA-001 - Design Basis Bjørnafjorden.

/2/ SBJ-01-C4-SVV-01-BA-001 - Metocean Design Basis.

/3/ NS-EN 1991-1-4:2005+NA:2009. Eurocode 1: Action on structures. Part 1-4: General actions – Wind actions

/4/ N400 Bruprosjektering. Statens Vegvesen.

/5/ Vurdering og sammenlikning av brukonsepter for kryssing av Bjørnafjorden. Oppetid. Versjon 1.0. 25.04.2016.

Concept development, floating bridge E39 Bjørnafjorden

Appendix E – Enclosure 8

10205546-08-NOT-176

Aerodynamic stability K11

MEMO

PROJECT	Concept development, floating bridge E39 Bjørnafjorden	DOCUMENT CODE	10205546-08-NOT-176
CLIENT	Statens vegvesen	ACCESSIBILITY	Restricted
SUBJECT	Aerodynamic stability of K11	PROJECT MANAGER	Svein Erik Jakobsen
TO	Ketil Aas-Jakobsen	PREPARED BY	Allan Larsen
COPY TO	Petter Sundquist	RESPONSIBLE UNIT	AMC

SUMMARY

This memo summarises the wind stability of the bridge girders of the K11 alternative for Bjørnafjorden bridge. Based on Håndbok N400 the bridge should be aerodynamically stable for speeds up to 81.7m/s.

The memo concludes that the K11 bridge is aerodynamically stable at wind speeds up to and beyond the requirements set by Håndbok N400 Bruprosjektering.

00	24.05.2019	Final issue	A. Larsen	K. Aas-Jakobsen	S. E. Jakobsen
REV.	DATE	DESCRIPTION	PREPARED BY	CHECKED BY	APPROVED BY

1 Wind load class

Following N400 /1/, section 5.4.3, a bridge shall be considered wind load class III when the following criteria apply:

- Highest eigen period > 2 s
- Span length > 300 m

Modal analyses of the K11 alternative for Bjørnafjorden floating bridge yields the highest eigen period to be 126 s. Further the main span of the cable stayed bridge is 380 m.

The above class III criteria are thus seen to be fulfilled. Hence verification of the wind stability of the bridge structure shall include interactions between the dynamics of the structure and wind field as well as aerodynamic stiffness and damping effects. The verification thus includes assessment of vortex induced vibrations /1/ section 5.4.3.7 and check of aerodynamic instabilities /1/ section 5.4.3.8.

2 Critical wind speed for onset of aerodynamic instabilities

Following N400 /1/, section 5.4.3 the critical wind speed for onset of aerodynamic instabilities shall be higher than 1.6 times the 500 year return period, 10 min mean wind speed at bridge girder level:

$$V_{crit}(z) > 1.6 \cdot V_m(z, T = 600\ s, R = 500\ year) \quad (1)$$

Following the MetOcean Design Basis /2/ the 50 year return period, 10 min mean wind speed at z = 10 m level is $V_m(z = 10\ m, T = 600\ s, R = 50\ year)$ = $V_{m,b}$ = 30.5 m/s.

Extrapolation to the level of the cable stayed bridge (z = 65 m) proceeds following (2):

$$V_m(z) = C_{prob} \cdot V_{m,b} \cdot k_T \cdot ln\left(\frac{z}{z_0}\right) \quad (2)$$

/2/ defines k_T = 0.17 and z_0 = 0.01 m for the Bjørnafjord site.

C_{prob} is a coefficient that transforms 50 year return wind speeds to other return periods R /3/:

$$C_{prob} = \sqrt{\frac{1 - 0.2 \cdot ln\left(-ln\left(1 - \frac{1}{R}\right)\right)}{1 - 0.2 \cdot ln\left(-ln\left(1 - \frac{1}{50}\right)\right)}} \quad (3)$$

For $R = 500$ (3) yields C_{prob} = 1.122. Taking z = 65 m, (1), (2) yields $V_{crit}(65) >$ **81.7 m/s.**

3 Bridge girder aerodynamic properties

The present evaluation of the aerodynamic stability of the K11 bridge alternative is based on discrete vortex computations of steady state wind load coefficients and Aerodynamic Derivatives (flutter coefficients) for the SS1-b cross section, Figure 3.1.

The steady state wind load coefficients obtained in /4/ are reproduced in Table 3.1.

Aerodynamic derivatives calculated for the non-dimensional wind speed range 2.5 < V/fB < 25 are shown in Figure 3.2

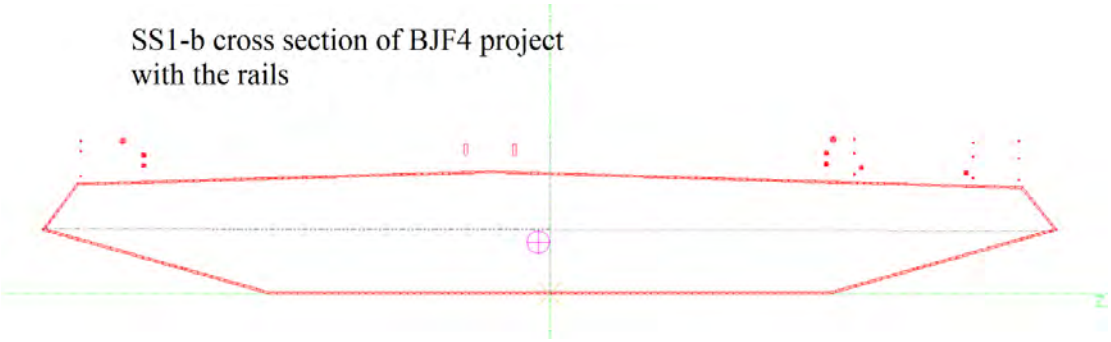

Figure 3.1 Discrete vortex panel model of the SS1-b cross section geometry.

Table 3.1 Steady state wind load coefficients for the SS1-b cross section from discrete vortex simulations.

C_{D0} [-]	C_{L0} [-]	$dC_L/d\alpha$ [1/rad]	C_{M0} [-]	$dC_M/d\alpha$ [1/rad]
0.57	-0.06	3.72	-0.013	0.93*

*$dC_M/d\alpha$ is estimated assuming the aerodynamic centre to be located at the upwind ¼ chord point

The wind load coefficients in Table 3.1 above are normalized the conventional way by the dynamic head of the wind ½ρV^2 and a characteristic dimension of the cross section. The section depth H = 3.5 m in case of the along wind drag loading and the cross section width B = 30 m in case of the lift and overturning moment.

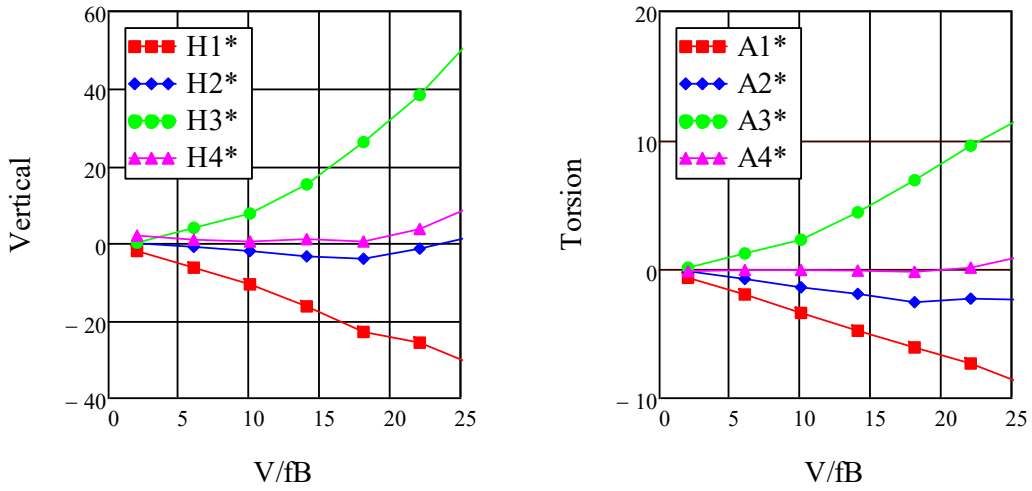

Figure 3.2 Aerodynamic derivatives for the SS1-b cross section from discrete vortex simulations.

The aerodynamic derivatives calculated at 6 discrete values of $(V/fB)_j$, $(j = 1 - 6)$ shown in Figure 3.2. The displays the expected behaviour for non-dimensional wind speeds in the range 2.5 < V/fB < 18 displaying a monotonic growth in a linear or parabolic fashion. For the highest non-dimensional wind speeds 18 < V/fB < 25 it is noted that the $H^*_{2..4}$ and $A^*_{2..4}$ aerodynamic derivatives display an unexpected non-monotonic behaviour which may influence stability calculations slightly.

4 Vortex induced vibrations

Vortex shedding in the wake of box girders may result in limited amplitude oscillations of the bridge girder at wind speeds where rhythmic vortex shedding locks on to a vertical bending or torsion eigen mode.

Practical experience from suspension bridges with shallow trapezoidal box girders have shown that vortex induced oscillations are usually confined to vertical modes only and occur at low wind speeds typically less than 12 m/s and for weather conditions with low atmospheric conditions.

Vortex induced vibrations of suspension bridges (Osterøy bridge, Norway and Storebælt East bridge, Denmark) has proven to be linked to severe flow separation and associated rhythmic vortex shedding at the knuckle line between the horizontal bottom plate and the lower inclined downwind side panel. Wind tunnel research /5/ has demonstrated that severe flow separation and vortex shedding can be avoided if the angle between the horizontal bottom plate and the lower side panels can be kept at approximately 15 deg. The 15 deg principle was recently introduced for the design of the girder of the Hålogaland Bridge, Norway and has proven to be free of vortex induced vibrations in full scale as well as in wind tunnel tests.

The design of the cross section shape of the girders of Bjørnafjorden bridge incorporates the 15 deg. principle. Thus, vortex induced vibrations are not expected to be an issue for the present design.

5 Verification of aerodynamic instabilities

N400 specifies that a wind load class III bridge shall be verified for four types of aerodynamic instabilities:

- Galloping
- Static divergence
- Classical flutter
- Torsion instability

Each type of aerodynamic instability will be discussed in separate sections below.

5.1 Galloping

Galloping is a cross wind vertical instability resulting in onset of vertical divergent oscillations above a certain threshold wind speed.

A necessary condition for galloping to occur is that the lift slope $dC_L/d\alpha$ is negative. With reference to Table 3.1 $dC_L/d\alpha$ = 3.72 > 0, thus galloping will not occur for the K11 design for Bjørnafjorden bridge.

5.2 Static divergence

Static divergence is a buckling type instability of the bridge girder occurring at the wind speed where the wind induced external moment acting on the girder exceeds the structural capacity. An estimate of the wind speed for onset for divergence V_{div} is given as /1/:

$$V_{div} = 2\pi f_\alpha \sqrt{\frac{2I_{\alpha eq}}{\rho B^4 \, dC_M/d\alpha}} \tag{4}$$

Where:

f_α is the eigenfrequency of the lowest torsion mode having modal mass M_α.

$I_{\alpha eq} = \frac{M_\alpha}{\int_0^L \varphi(x)^2 dx}$ is the corresponding equivalent mass moment of inertia.

ρ = 1.25 kg/m³ is air density

B = over-all girder width

The lowest torsion mode of the bridge is mode 25 displaying three half waves along the low level floating bridge, Figure 5.1, having an eigenfrequency f_α = 0.157 Hz and a modal mass M_α = 107.213·10⁶ kg.

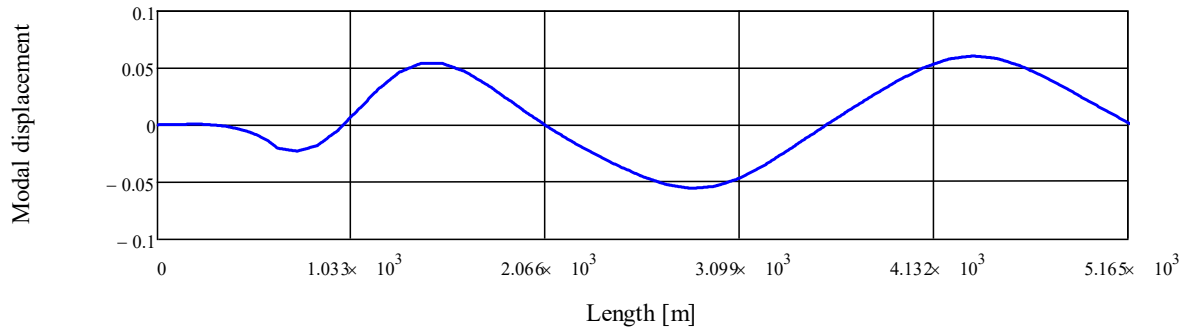

Figure 5.1 First torsion mode (mode 25) of Bjørnafjord K11 Alternative.

Inserting $dC_M/d\alpha$ = 0.92 and the above structural properties in (4) a divergence wind speed V_{div} = 2627 m/s which is well above the requirement of 81.7 m/s.

5.3 Classical flutter

Classical flutter involves as a minimum two modes of motion. A torsion mode and a vertical bending mode of similar mode shape but with a lower eigenfrequency. The critical wind speed for onset of classical flutter is reached when the wind loading on the bridge girder makes the bending and torsion frequencies equal thereby establishing a resonant exchange of energy between to two modes. This in turn leads to divergent coupled torsion bending oscillations of the bridge girder. In cases where more vertical modes exist below the torsion mode these vertical modes may couple to form a compound vertical mode shape which couples with the torsion mode at the onset of flutter.

Different methods exist for calculation of the flutter wind speed of a bridge deck. The present method outlined in section 6 is an expansion of the AMC method (Air material Command) which allows an arbitrary number of modes and degrees of freedom of a bridge deck to couple into flutter /6/. The input to the flutter calculation constitutes the modes assumed to couple into flutter, the corresponding modal masses and eigenfrequencies and aerodynamic derivatives particular to the bridge deck.

The present multi-mode flutter analysis of Bjørnafjorden K11 alternative assumes that the first torsion mode and 9 vertical bending modes may couple into flutter, Figure 5.3. Eigenfrequencies and modal masses with of the modes are listed in Table 5.1.

From the resulting flutter diagrams Figure 5.2 it is noted that all apparent damping levels remain negative for all wind speeds below 120 m/s. Hence the bridge is stable against classical flutter up to and beyond the N400 requirement of 81.7 m/s regardless of structural damping.

Table 5.1 Lowest vertical and torsion modal masses and eigenfrequencies. Bjørnafjord K11 alternative.

	Mode 14	Mode 15	Mode 16	Mode 17	Mode 18
Modal mass [kg]	$35723 \cdot 10^3$	$21048 \cdot 10^3$	$28676 \cdot 10^3$	$69297 \cdot 10^3$	$75426 \cdot 10^3$
Eigenfrequency [Hz]	0.1596	0.1538	0.1546	01548	0.1548
	Mode 19	Mode 20	Mode 21	Mode 22	Mode 25
Modal mass	$60315 \cdot 10^3$	$98445 \cdot 10^3$	$53534 \cdot 10^3$	$75942 \cdot 10^3$	$107213 \cdot 10^3$
Eigenfrequency [Hz]	0.1548	0.1548	0.1550	0.1550	0.1567

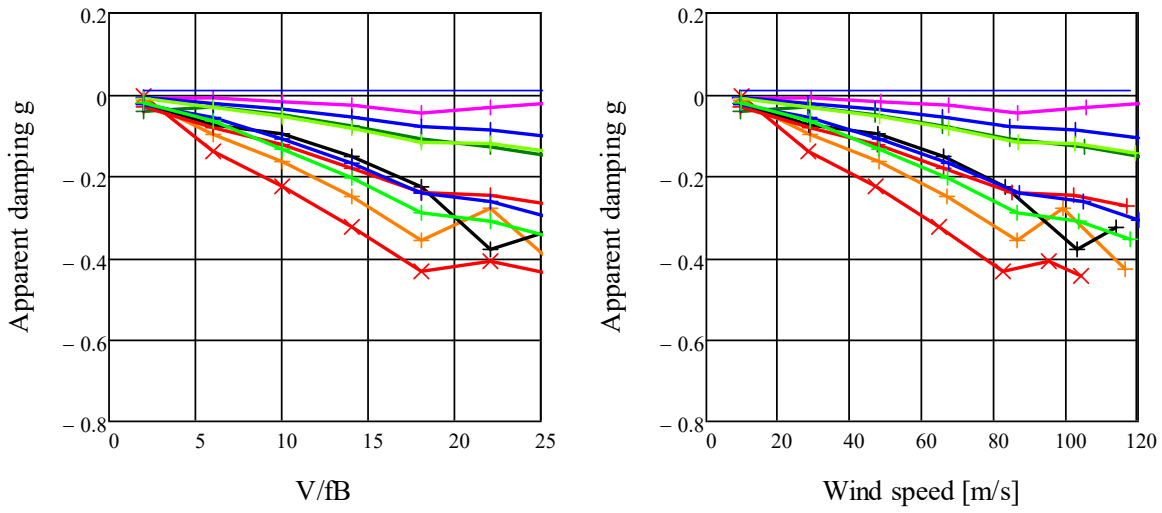

Figure 5.2 Apparent aerodynamic damping g as function of normalized and absolute wind speed for Bjornafjorden K11 alternative.

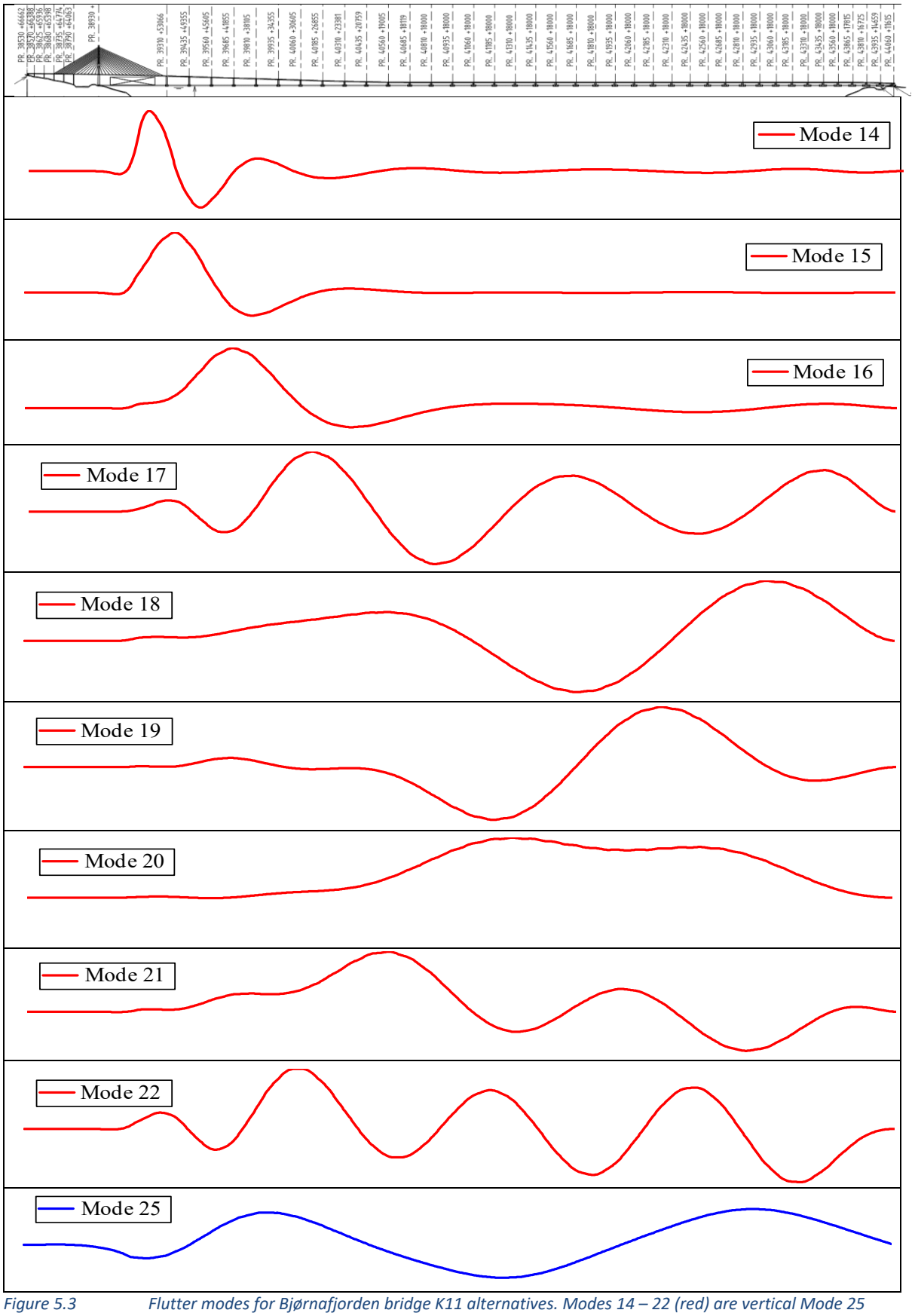

Figure 5.3 Flutter modes for Bjørnafjorden bridge K11 alternatives. Modes 14 – 22 (red) are vertical Mode 25 (blue) is torsion.

5.4 Torsion instability

Torsion instability is a condition resulting in onset of torsional divergent oscillations above a certain threshold wind speed. Torsion instability is associated with the formation and travel of large coherent vortex structures across the bridge deck /6/. This type of instability is often associated with bluff plate girder bridge decks.

A necessary condition for the occurrence of torsion instability is that the A_2^* aerodynamic derivative change sign from negative at low wind speeds to positive at higher wind speeds.

From Figure 3.2 it is noted that A_2^* remains negative for all non-dimensional wind speeds up to at least V/fB = 25. It may thus be concluded that Bjørnafjorden K11 alternative will not encounter torsion instability at wind speeds below a wind speed of 25· $f_\alpha B$ = 117 m/s which is well above the N400 requirement.

6 Multimode flutter theory

The calculation of the critical wind speed for onset of flutter follows from solving the complex valued eigenvalue problem (5) which combines the modal and aerodynamic properties of one torsion mode $\alpha(x)$ and n vertical bending modes $h1(x)$ … $hn(x)$, /6/.

$$Det\begin{bmatrix} 1 + A_{\alpha\alpha,j} - \lambda_{1,j} & \cdots & A_{\alpha hn,j} \\ \vdots & \ddots & \vdots \\ H_{hn\alpha,j}\left(\frac{f_\alpha}{f_{hn}}\right)^2 & \cdots & \left(1 + H_{hnhn,j}\right)\left(\frac{f_\alpha}{f_{hn}}\right)^2 - \lambda_{n,j} \end{bmatrix} = 0 \tag{5}$$

The individual elements in (5) combine modal and aerodynamic characteristics of the bridge deck girder and are composed as follows:

$$\begin{aligned} A_{\alpha\alpha,j} &= \frac{\rho B^4}{M_\alpha} C_{\alpha\alpha}\left(A_{3,j}^* + iA_{2,j}^*\right), & C_{\alpha\alpha} &= \int_0^L \alpha(x)^2 dx \\ A_{\alpha hn,j} &= \frac{\rho B^4}{M_\alpha} C_{\alpha hn}\left(A_{4,j}^* + iA_1^*, j\right), & C_{\alpha hn} &= \int_0^L \alpha(s) hn(x) dx \\ H_{hn\alpha,j} &= \frac{\rho B^2}{M_{hn}} C_{\alpha hn}\left(H_{3,j}^* + iH_{2,j}^*\right), & C_{hn\alpha} &= \int_0^L \alpha(s) hn(x) dx \\ H_{hnhn,j} &= \frac{\rho B^2}{M_{hn}} C_{hnhn}\left(H_{4.j}^* + iH_{1.j}^*\right), & C_{hnhn} &= \int_0^L hn(x)^2 dx \end{aligned} \tag{6}$$

The unknown to be solved for is the flutter frequency f which is embedded in the eigenvalues $\lambda_{n,j}$ through the identity:

$$Re\left(\lambda_{n,j}\right) + i\, Im\left(\lambda_{n,j}\right) = \left(1 + ig_{n,j}\right)\left(\frac{f_\alpha}{f}\right)^2 \tag{7}$$

Where $g_{n,j}$ is the apparent aerodynamic damping (negative) of a given mode at a given non-dimensional wind speed V/fB_j.

Once the complex eigenvalues $\lambda_{n,j}$ are determined for each of the non-dimensional wind speeds $V/fB_j = V_j^*$ for which the flutter derivatives are available, the equivalent aerodynamic damping and corresponding wind speed are obtained as:

$$g_{n,j} = \frac{Im(\lambda_{n,j})}{Re(\lambda_{n,j})}, \qquad V_j = V_j^* \frac{f_\alpha B}{\sqrt{Re(\lambda_{n,j})}} \tag{8}$$

By plotting the equivalent aerodynamic damping g as function of the wind speed the critical wind speed is identified where the apparent damping $g_{n,j}$ equals twice the structural damping:

$$g_{n,j} = 2\zeta \tag{9}$$

6.1 Example, critical wind speed of Storebælt East Bridge

The above procedure is illustrated in the example below which pairs the aerodynamic derivatives shown in Figure 3.2 with the structural properties of Storebælt East bridge section model (unity modes along the span) for which wind tunnel measurement of the critical wind speeds are reported in the literature /7/.

Storebælt East bridge section model structural data (two modes):

Mass / unit length: m = 22.74·10^3 kg/m

Mass moment of inertia / unit length: I = 2.47·10^6 kg/m

Vertical bending frequency: f_h = 0.1 Hz

Torsion frequency: f_α = 0.278 Hz

Deck width: B = 31 m

Structural damping: ζ = 0.003

Determination of the critical wind speed for onset of flutter following the above method is shown in Figure 6.1. It is noted that the red branch remains negative for all wind speeds. The purple branch starts being negative at low wind speeds but intersects the blue horizontal line (twice the structural damping) at a non-dimensional wind speed at V/fB = 12.3 (left diagram) corresponding to a critical wind speed of about 79 m/s (right diagram) which may be compared to a critical wind speed in the range 70 – 74 m/s measured in the wind tunnel /7/.

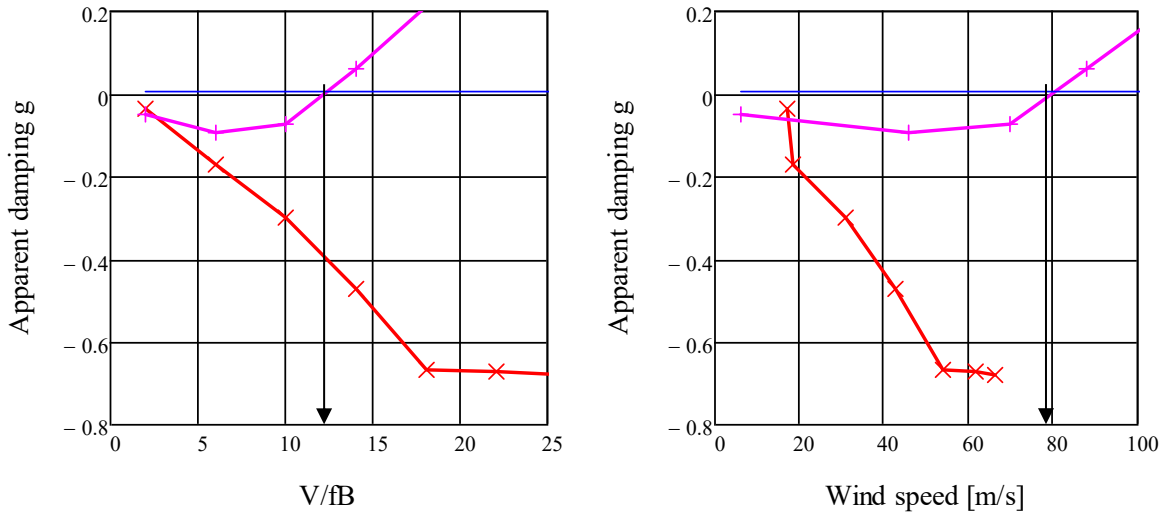

Figure 6.1 Determination of the critical wind speed for onset of flutter in non-dimensional for (left) and actual wind speed (right). Example: Storebælt East Bridge dynamic properties paired with SS1-b aerodynamic dericatives.

The geometry of the Storebælt East bridge and the SS1-b cross section is not identical, thus a perfect match of the above flutter calculation and the Storebælt wind tunnel tests can not be expected. However, the relatively close match is quite satisfactory and supports the credibility of the computed aerodynamic derivatives.

7 References

/1/ N400: Håndbok, Bruprojektering, Statens vegvesen

/2/ MetOcean Design Basis. Document nr.: SBJ-01-C4-SVV-01-BA-001, 14-11-2018 including addendum of 18-03-2019.

/3/ Eurocode 1: Action on structures – Part 1-4: General actions – Wind actions. 2ed, 2007.

/4/ Memo 10205546-08-NOT-062: CFD analysis of cross section.

/5/ Larsen, A., Wall, A.: Shaping of bridge box girders to avoid vortex shedding response. Journal of Wind Engineering and Industrial Aerodynamics 104-106, (2012) 159-165.

/6/ Larsen, A.: Bridge Deck Flutter Analysis. Proceedings of the Danish Society for Structural Science and Engineering, Vol. 87, No. 2-4, 2016.

/7/ Larsen, A.: Aerodynamic aspects of the final design of the 1624 m suspension bridge across the Great Belt. Journal of Wind Engineering and Industrial Aerodynamics 48, (1993) 261-285.

AAS-JAKOBSEN COWI Multiconsult

JOHS HOLT AkerSolutions entail NGI DISSING+WEITLING architecture a|s mossmaritime

Concept development, floating bridge E39 Bjørnafjorden

Appendix E – Enclosure 9

10205546-08-NOT-183

Inhomogeneity in wind – effects on K12

INTERNAL - MEMO

PROJECT	Concept development, floating bridge E39 Bjørnafjorden	DOCUMENT CODE	10205546-08-NOT-183
CLIENT	Statens vegvesen	ACCESSIBILITY	Restricted
SUBJECT	Inhomogeneity in wind – effects on K12	PROJECT MANAGER	Svein Erik Jakobsen
TO	Statens vegvesen	PREPARED BY	Ketil Aas-Jakobsen
COPY TO		RESPONSIBLE UNIT	AMC

SUMMARY

This note shows results from calculation of dynamic transverse response due to wind for concept K12, for four different variations of wind speed along the alignment. Results of variations of the parameters found in Table 15 in the Metocean Design basis is also shown. For the different distributions of the wind speed along the alignment, the case with constant distribution gives the highest dynamic wind response for all directions. Dynamic wind response of xLu, Au, Cux and Cuy is calculated and compared to N400 values. K12 is most sensitive to change in Cuy when the wind is more or less perpendicular to the alignment. For wind in the sector along the alignment the response is less sensitive to change of the calculated parameters.

0	15.08.2019	Final issue	K. Aas-Jakobsen	R. M. Larssen	S. E. Jakobsen
REV.	DATE	DESCRIPTION	PREPARED BY	CHECKED BY	APPROVED BY

Table of Contents

1 Introduction

Several floating bridge concepts are proposed for the Bjørnafjorden crossing. This document explore the effect of inhomogeneity in wind the K12 concept, which is the curved bridge with side anchors.

The main focus will be on inhomogeneity effects on dynamic response for K12. K12 is a curved in the horizontal plane and transverse force is carried by the its shape and additional side anchors. The concept is illustrated in Figure 1.

The calculations are done with a simplified, but fast method capable of varying input parameters including wind from all angles and variation of mean wind along the alignment. Results are presented as standard deviations of transverse displacement and strong axis moment. The basic idea is to utilise the eigenmodes of the structure to calculate the response and sum the modal response over all relevant modes. This is a well proven method for calculating dynamic response from wind. However, the simplified method has several disadvantages; currently it has a simplified load model implemented, it does not currently handle geometric stiffness, and damping introduced through the wetted part of the structure is introduced as static modal values for each mode, calculated for the base case with wind perpendicular to the structure. A simplified model is used to adjust the damping for different direction of the wind.

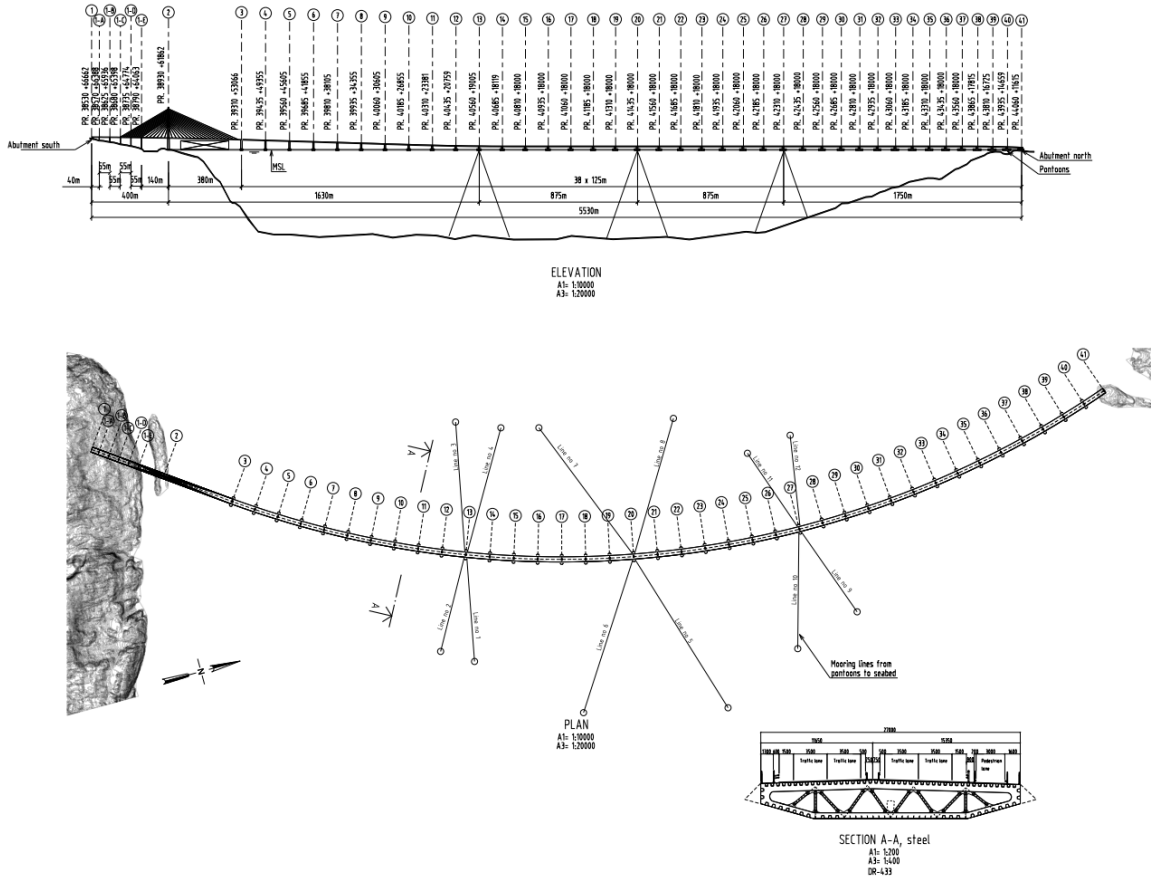

Figure 1 K12 General arrangement.

2 Implementation – calculation of displacement

2.1 Calculation of displacement

Calculation of dynamic response from wind is simplified by including only the resonant part. I.e. the background part is discarded. For lightly damped structures calculations in other projects have shown that this will underestimate the dynamic response with about 5-10%.

The formulation in Eq. 6.50 in /6/ is used for calculating modal response:

$$Q(f_e) = \rho \sum_i^L \sum_j^L \sqrt{(C_D H V)_i \; S_u(x_i, f)(C_D H V)_j \; S_u(x_j, f_e)} \sqrt{coh(f_e, \Delta s)} \varphi_i \varphi_j \qquad (1)$$

Where f is the eigenfrequency of the mode and C_D, H, V, S_u and φ is evaluated individually for every element, and √coh is based on the separation of the point and the associated mid-point value.

The standard deviation for the response of each modes is obtained by

$$\sigma_y(f_e) = \sqrt{\frac{\frac{\pi f_e}{4\zeta_m} Q(f_e)}{(2\pi f_e)^4 M_m^2}} \qquad (9)$$

Where f_e, M_m, and ζ_m are modal values for the particular mode. For ζ_m the structural damping is given as input and the aerodynamic damping is calculated. Viscous and hydrodynamic modal damping from the pontoons and line damping are taken from a separate analysis where the wind is perpendicular to the alignment. In order to compensate for different damping levels of viscous and line damping for different angle of attack, an empirical formula for compensation was developed in another part of this project, based on comparison with Orcaflex results. The formulae and principle is shown in Figure 2.

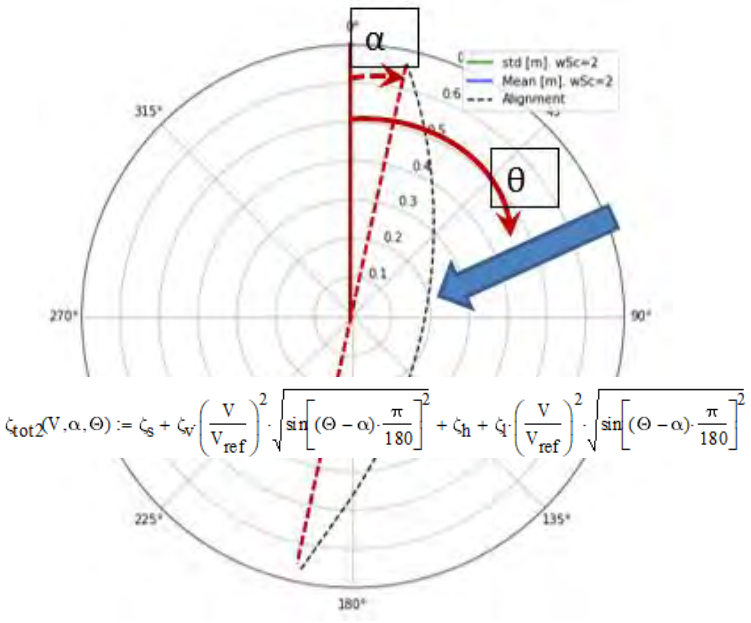

Figure 2 Empirical adjustment of damping.

The overall response of the included modes is calculated by the Root-Square-Sum method. Typically, 20 modes is included. Moment values are calculated by differentiation.

Results are presented in a polar diagram similar to the one shown in Figure 3. The angle in this diagram reflects the direction the wind is coming from. 0 degrees is wind from north and 90 degrees is wind from East. A sketch of the alignment is shown as a broken black line.

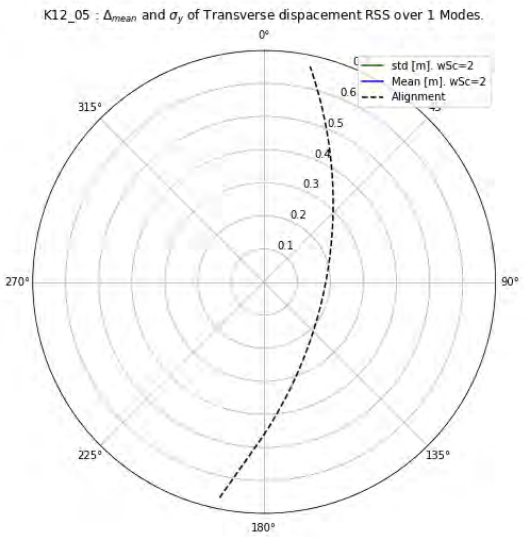

Figure 3 Principles for response presentation.

2.2 Analysis input parameters - wind

The analysis was conducted for wind response only. It was selected to use wind speed with 100year return period and as a first step it was selected to calculate response with the same turbulence intensity for all directions. Thus, standard N400 formulas and values are used in these reference calculations and the wind input to the analysis is:

Basic wind speed at z=10m : vb=25.2m/s
Surface roughness: z_0=0.01
Length scale at z=10m: $^{x}L_u$=100m
Spectral shape parameter: A_u=6.8
Decay parameters: C_{ux}=3, C_{uy}=10, C_{uz}=10,

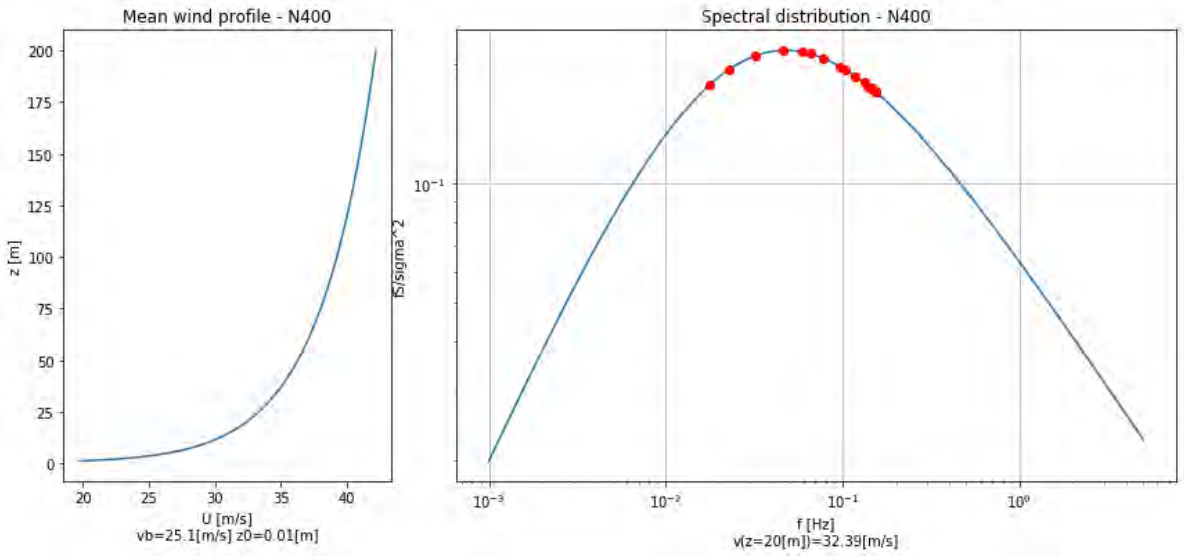

Figure 4 Left: Mean wind profile. Right: Spectral distribution with first 20 modes indicated (K12).

2.3 Analysis input parameters – structural

The analysis mode is imported from a master sheet which also is used to build the Orcaflex model. Thus, the geometry is the same as used in the Orcaflex analysis. Modal properties are derived from a NovaFrame analysis with the same structural and geometric properties. This analysis also estimates hydrodynamic, viscous, aerodynamic and line damping for each mode.

Structural damping is generally set to the target value of 0.5% of critical. Since Orcaflex implements damping as Rayleigh damping, it is also implemented in this way in these calculations. The Rayleigh damping for the Orcaflex model is set to the target values for a low and high frequency. Due to the nature of Rayleigh damping the structural damping used in the current calculation is lower than the target value i.e. conservative.

Model used in calculations in this report: K12-06

The simplified load model used in these calculations only take into account the drag loading (See equation (1)). For simplicity C_D is extracted for zero angle of attack. The values used for the high and low bridge, Figure 5 and Figure 6, is given in Table 1. In addition drag contributions from columns and cable stays are added at the correct location. Thus, the average Cd of the system is 0.88.

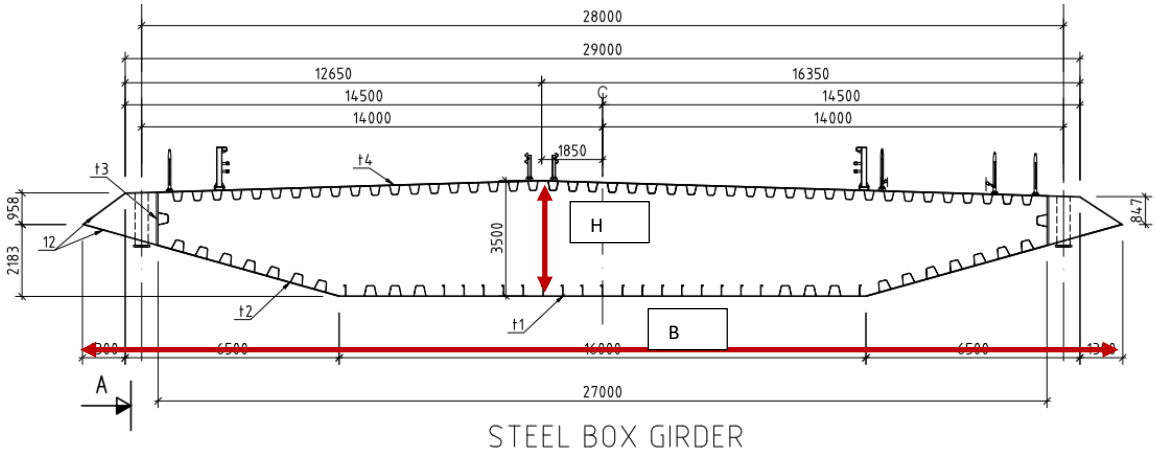

Figure 5 High bridge girder

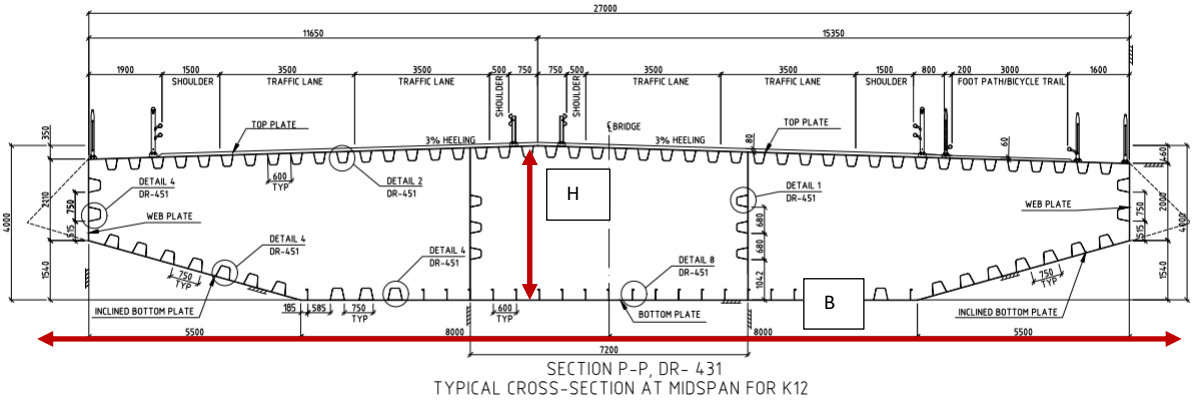

Figure 6 Low bridge girder

Table 1 Wind load parameters used in calculations.

	H [m]	**B** [m]	**C_D**	**dC_D** [1/rad]	**C_L**	**dC_L** [1/rad]	**C_M**	**dC_M** [1/rad]
High bridge	3.5	30.2	0.67	0.0	0.0	0.0	0.0	0.0
Low Bridge	4.0	30.2	0.80	0.0	0.0	0.0	0.0	0.0

2.4 Modes

No of modes used in calculations: 20 (T1=56.8s – T20=6.48s) is shown in Figure 7. Each plot shows transverse modal displacement as red, vertical modal displacement as green and torsional modal rotation as blue. Torsional contribution is scaled up by a factor of 10 to be visible on the plots as can be seen the transverse response dominates the first 14 modes.

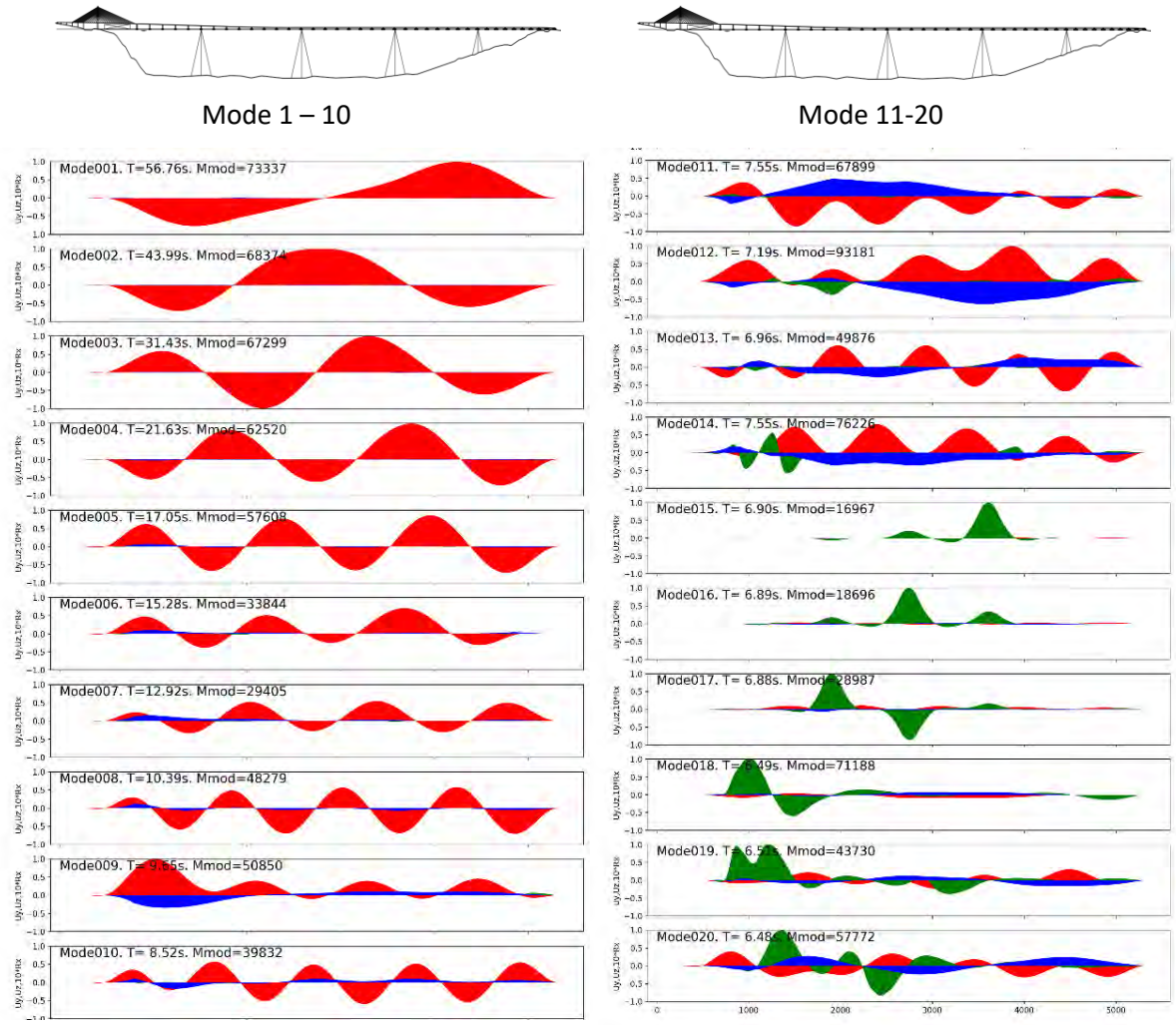

Figure 7 Modeplot of first 20 modes of K12_06. Red: Transverse direction, Green: Vertical direction. Blue: torsional component scaled by a factor of 10.

2.5 Load model

Currently, only a simplified load in the drag direction is implemented in this method, which only takes into account the fluctuating u-component of the wind. Skew wind is include by a decomposition of the force as shown below. When developing the method further more advanced load models can be implemented. The following load model is used:

$F_D = 1/2*\rho*(C_D* \cos(\alpha))*H*U^2$

3 Verification of calculation method.

A flexible python script is developed based on the method described in Section 2.1 and checked versus hand-calculations (Mathcad) and full time-domain simulations in Orcaflex before parameter variations are reported.

3.1 Verification versus hand-calculations

The method described in Section 2.1 is implemented in a Mathcad sheet, see Appendix A. Modal parameters and damping values are imported from Excel sheets. These sheets contain the same modal values as the ones used in the Orcaflex analysis.

The Mathcad sheet only takes into account wind on the girder. Since the Python script also takes into account wind area on cables and columns, an average Cd values is calculated from the Python input and used in Matchad. The weighted average value of the drag coefficients is 0.88 in Python, thus this value is used in the verification.

Mode-by-mode transverse displacement is calculated both in Mathcad and Python and compared for the case with mean wind perpendicular to the main alignment axis. Result comparison of standard deviation of transverse displacement is give in Table 2. As can be seen, the comparison is good both mode-by-mode and RSS over the 5 modes.

Table 2 Comparison of Mathcad and Python script for K12_06. Transverse displacement.

Mode	Frequency [Hz]	Total damping [% of crit]	Mathcad – std [m]	Python – std [m]
1	0.018	3.400%	0.930	0.927
2	0.023	3.955%	0.517	0.533
3	0.032	1.988%	0.322	0.315
4	0.046	1.593%	0.145	0.138
5	0.117	4.167%	0.107	0.096
		RSS	1.126	1.127

Figure 8 shows a comparison along the alignment between Mathcad and Python, which shows that the agreement is good.

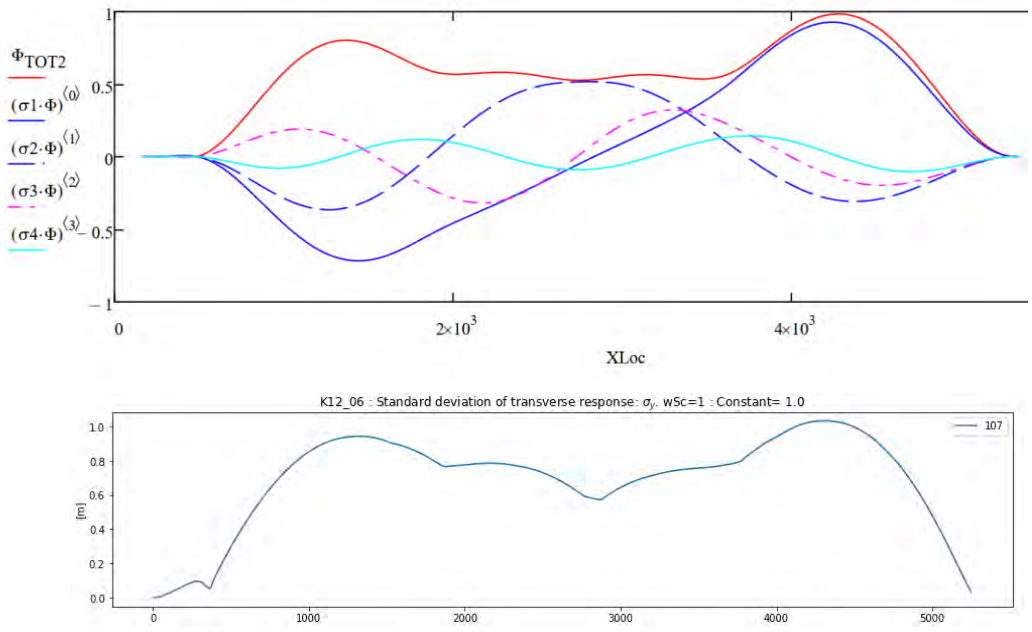

Figure 8 Comparison along alignment. Top: Matchad. Bottom: Python script.

3.2 Verification versus Orcaflex

Verification of the simplified method was done my matching results with Orcaflex for the same input values. Orcaflex calculates the response in the time domain, and are thus, able to include non-linear effects of loading and response. Since Orcaflex has been verified and benchmarked with other calculation codes its reference for this verification.

The simplified method is based on a frequency domain approach, which is significantly faster than the time domain approach used by Orcaflex, but is not capable of handling nonlinearities in e.g. hydrodynamics and aerodynamics, thus, exact match of results are not expected. Results of the comparison are shown in Figure 9. The left figure shows the standard deviation of the displacement, while the right figure shows the calculated strong axis moment. Red dots are Orcaflex values (average of 10 runs), while the blue thick line is results from the simplified method for all wind angles and the doted lines indicate +/- 10% of the simplified method.

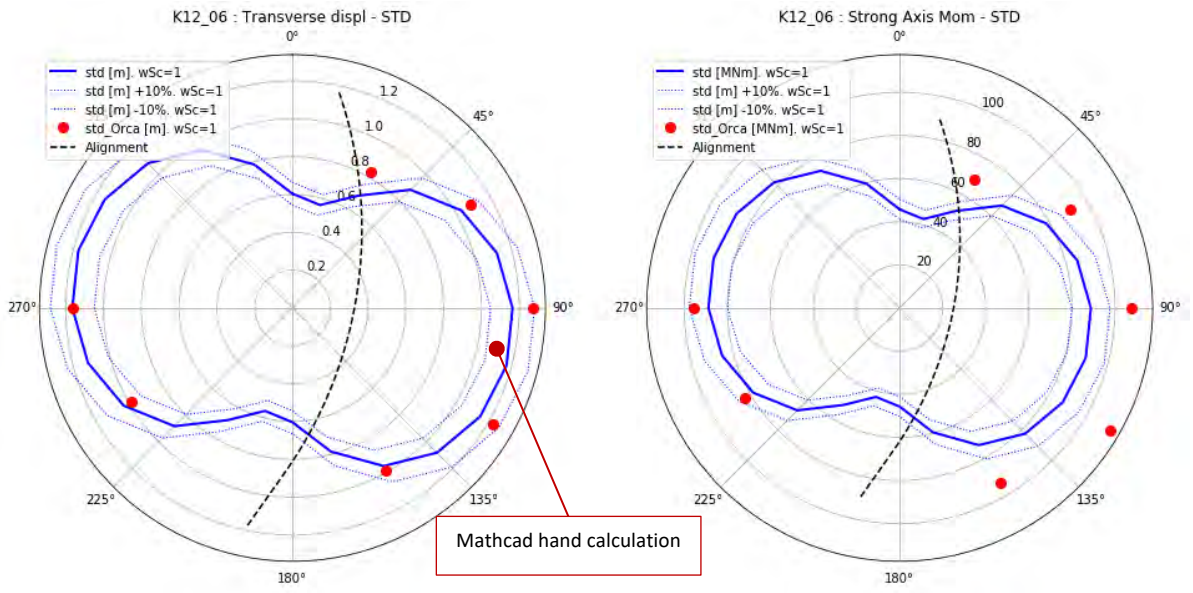

Figure 9 Comparison of standard deviation between simplified method and Orcaflex.
Blue solid line: Simplified method
Blue dotted lines: Simplified method +/- 10%.
Red dots: Orcaflex (average of 10 runs).
Black broken line: Alignment of K12.

The main purpose of this note is to study the effects and trends of varying wind parameters. Thus, the most important part of the comparison is to see that the simplified model is able to follow the major trends of the Orcaflex calculations.

Displacement results

For wind from east that are close to perpendicular to the alignment good agreement is found on comparison of displacement, while the results deviate more for wind from north and south. For wind from west the displacement shows good agreement. There are some differences in the physics that the models are able to represent that may contribute to the differences.

Possible sources for the deviations are:

- The simplified Python script uses the eigenfrequency only, and thus, discards the background value. Orcaflex uses all load frequencies in response calculations and thus includes the background response. Inclusion of background response will increase the response compared to using only the resonant part. A simplified analysis estimates the background response to about 6% on the standard deviation for the first mode of this structure, see the appendix for calculation.

- Effects of geometric stiffness that slightly changes the vibration frequencies, which again changes how the structure attracts load from the surroundings. This geometric effect is automatically included in Orcaflex, while not included in the modal input in the simplified frequency domain analysis. This is consistent with wind from east increasing the compression in the arc, thus reducing the stiffness, which leads to reduced frequency, and thus, increased response. A simplifed sensitivity study on the above example gave a 7% increase of response for a 3% reduction of vibration frequencies (i.e. softening due to compression in the members).

Strong axis moment

For the strong axis moment the simplified model follows the trend of Orcaflex for all checked wind attack angles. It is noted that larger deviations are found here than for displacement and that the simplified model underestimate the strong axis moment. This is most likely due to a more coarse segmentation of the simplified model, thus not resolving the curvature with the precision needed to get accurate results.

Even though the accuracy of this simplified method is not good enough for design, it is considered good enough for the purpose of this analysis; to look at the effect and differences in response for varying wind.

4 Analysis and Results

4.1 Introduction

The following pages shows maximum transverse displacement as standard deviation for all wind directions for each wind scale types (Root Square Sum values). Results are plotted against the case with uniform wind along the alignment and with standard N400 values. Only wind from the easterly direction is calculated, as the verification calculations (above) showed a fairly symmetric response pattern along the mean alignment.

The following legends is used:
Blue solid thick line: Reference value (Results with N400 values)
Blue dotted lines: Reference value +/- 10%
Black broken line : alignment of the concept.
Colored lines: result from parameter variation.

4.2 Mean wind variation along the alignment

Figure 10 describes and shows the variation of mean wind along the alignment. The left part of the figure represent the mean wind in the south end of the structure, while the right part of the figure represent the wind in the north end of the structure.

wScaleType	Shape
wScaleType=1 wMin=1;wMax=1 Constant=1.0	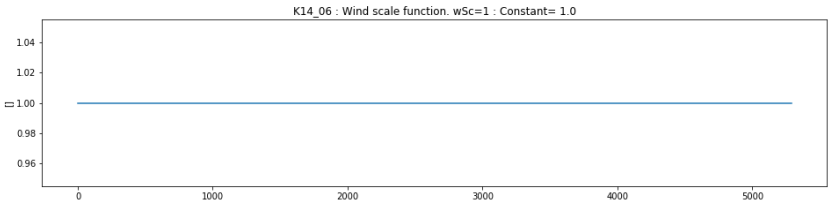
wScaleType=2 wMin=0.6;wMax=1.0 Linear 0.6->1.0	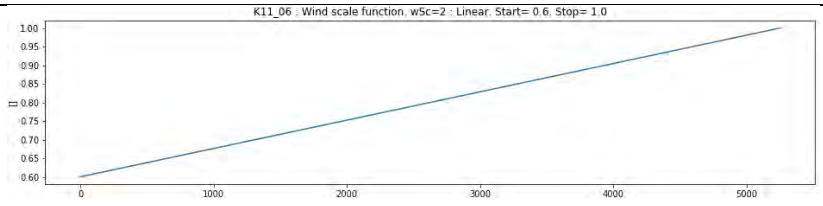
wScaleType=3; wMin=1.0;wMax=0.6 Linear 1.00->0.6	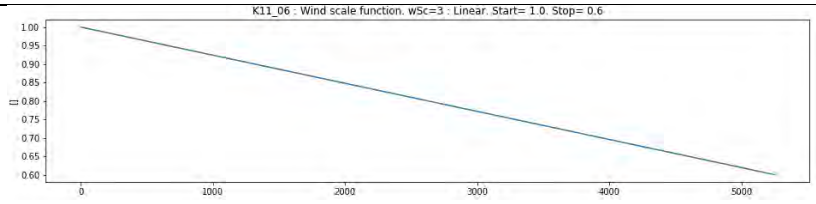
wScaleType=4; wMin=0.8;wMax=1.0 Bi-linear (mid peak): 0.8->1.0->0.8	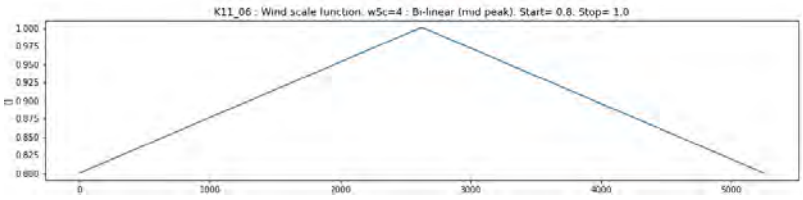

Figure 10 Wind variation along the alignment.

A summary of the results is shown in Figure 11. As can be seen the general trend is that constant mean wind (Wind Scale Type 1) gives the highest dynamic response regardless of direction. Second largest effect is from Wind Scale Type 4. Both these cases is symmetric about the mean. The two

remaining Wind Scale Types are un-symmetric, and the maximum of the two is dependent on the direction of the wind in relation to the structure.

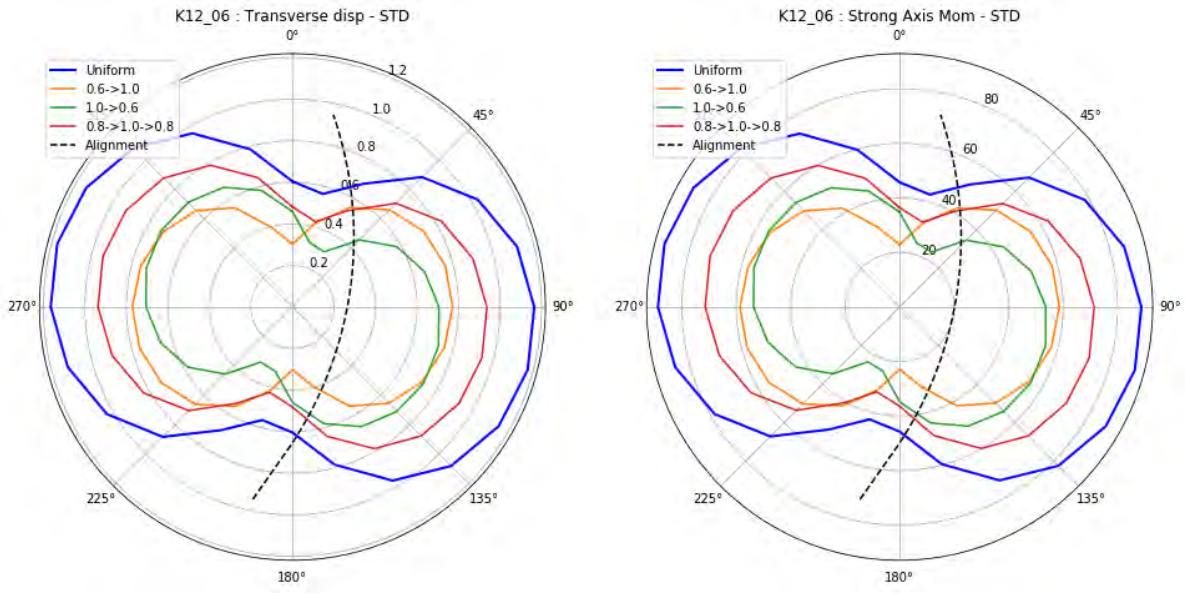

Figure 11 Dynamic response from varying mean wind profile along the deck, see Figure 10. The variation is from south towards north. I.e. for the yellow line the mean wind varies from 0.6 in the south to 1.0 in the north.

4.3 Variation in Table 15

4.3.1 Introduction

In Metocean Design basis /2/ Table 15 indicate that parameters in the wind varies. The key parameters are presented as P-values, representing probability of occurrence lower than the specified value. In orderer to understand the effect og the variation several relevant parameters were calculated and compared to the reference value; uniform wind as documented in Section 4.2. Table 3 gives the variations used.

*Table 3 Extract from "Table 15". Input varied below marked with blue.*Cux not given in N400. ESDU value is used in reference calculations.*

		Metocean Design Basis			Analysis input (z=10m) (scaled based on N400)		
	N400	**P10**	**P50**	**P90**	**P10**	**P50**	**P90**
z [m]	10,0	50,0	50,0	50,0	10,0	10,0	10,0
xLu [m]	100,0	108,0	232,0	586,0	66,6	143,2	361,6
xLv [m]	25,0	50,0	141,0	472,0	30,9	87,0	291,2
xLw [m]	8,3	21,0	40,0	81,0	13,0	24,7	50,0
Au	6,8	3,80	7,30	16,30	3,8	7,3	16,3
Av	9,4	5,60	13,30	32,50	5,6	13,3	32,5
Aw	9,4	7,70	12,30	18,20	7,7	12,3	18,2
Cux*	3,0	-	-	-	5,0	7,0	10,0
Cuy	10,0	6,40	9,00	10,8	6,40	9,00	10,8

4.3.2 Variation of xLu

For variation of xLu the response follows the reference value within +/- 10%. Low and high xLu values give lowest response. The results indicate that the highest response value for this concept is for an xLu value in medium range.

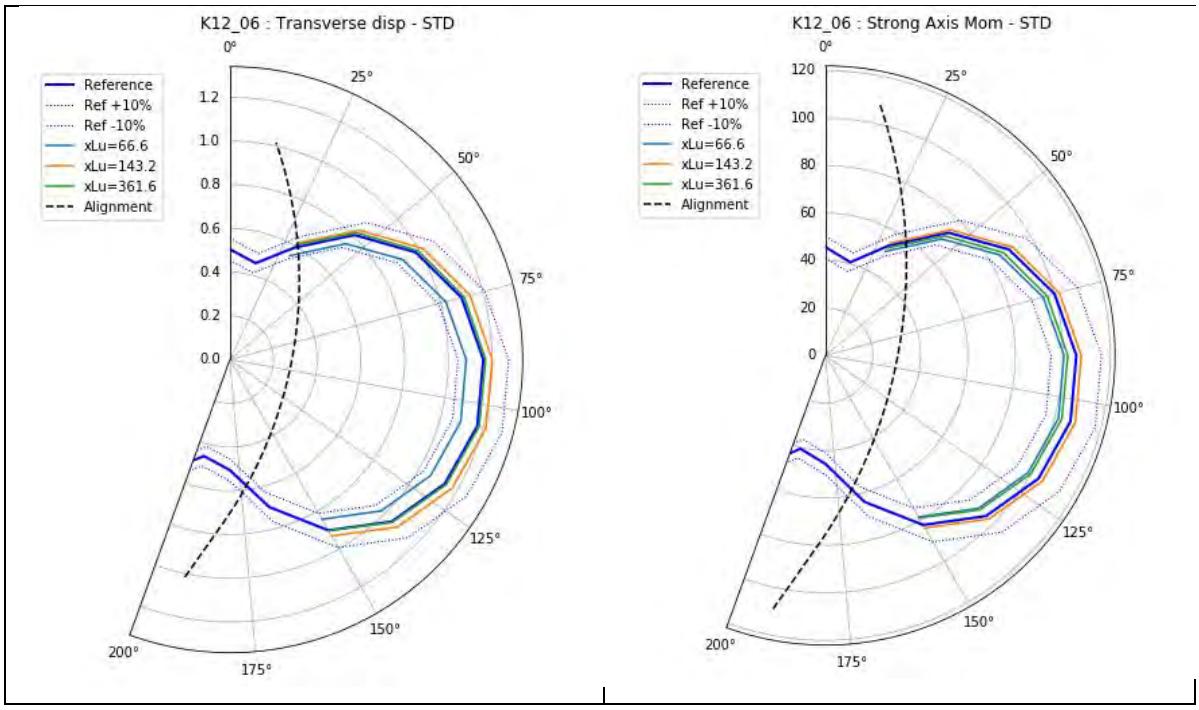

Figure 12 xLu variation. Left: std of displacement. Right: std of strong axis moment.

4.3.3 Variation of Au

For variation of Au the response follows the reference value within +/- 10%. The general trend is that increased Au values gives increase response.

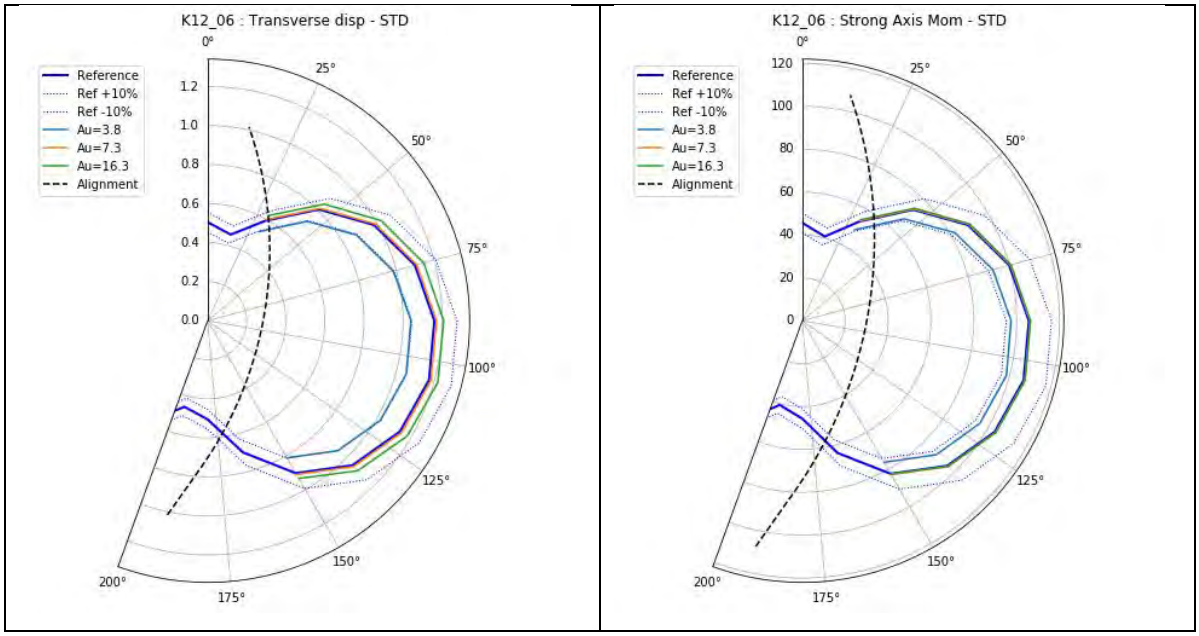

Figure 13 xLu variation. Left: std of displacement. Right: std of strong axis moment.

4.3.4 Variation of Cux

For variation of Cux the response follows the reference value within +/- 10%. The effect of change of cux is small for wind perpendicular to the alignment and more pronounced as the wind comes along the alignment. The Cux value of 3.0 used in the reference case gives the highest value of the calculated cases and increase of Cux value give reduced response.

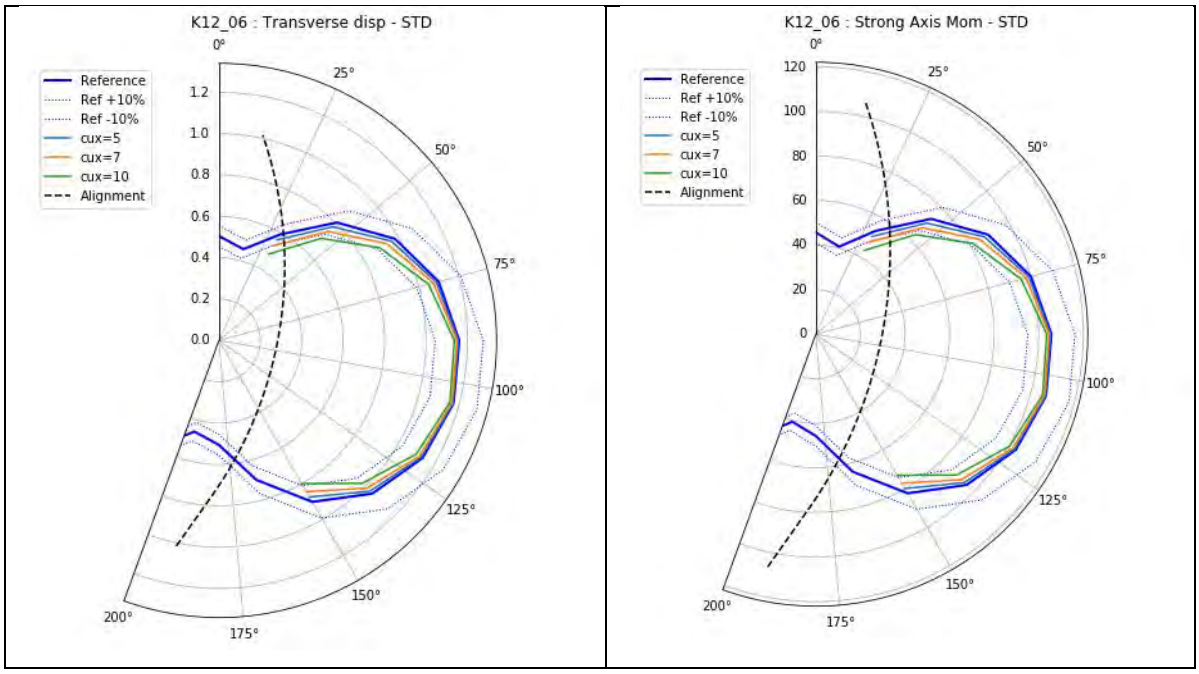

Figure 14 xLu variation. Left: std of displacement. Right: std of strong axis moment.

4.3.5 Variation of Cuy

The calculation of variations of Cuy is shown in Figure 15. As can be seen the response is sensitive to change of Cuy, particularly for wind perpendicular to the alignment. Lower value of Cuy gives higher response and Cuy values below the P10 value of 6.4 increases the response with more than 20%. For skew wind, where the wind is more along the alignment, the effect is less pronounced.

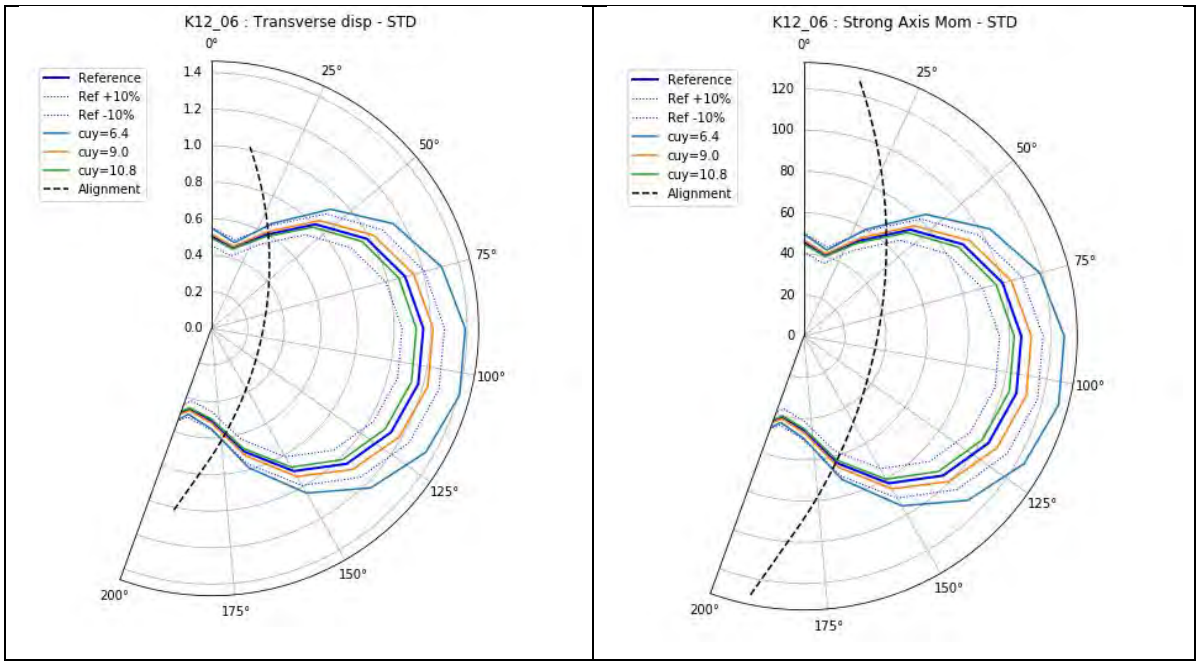

Figure 15 Cuy variation. Left: std of displacement. Right: std of strong axis moment.

5 Results and Discussion

Wind response of K12 for N400 standard wind values is calculated with a simplified method. The model is extracted from Orcaflex and contain the same modal parameters and damping, including hydrodynamic effects. The simplified method is compared to hand calculations and Orcaflex and shows fairly good agreement.

For the different distribution of the wind speed along the alignment, the case with constant distribution gives the highest dynamic wind response for all directions.

Sensitivity within the P10-P90 values is compared to the values given in N400. Of the studied parameters, xLu, Au, Cux and Cuy, Cuy gives the largest difference compare to N400.

For wind more or less perpendicular to the alignment Cuy gives the largest changes compared to N400 values. For wind along the alignment the sensitive to change is larges for Cux, but small in general.

6 References

/1/ SBJ-32-C4-SVV-90-BA-001 - Design Basis Bjørnafjorden.

/2/ SBJ-01-C4-SVV-01-BA-001 - Metocean Design Basis.

/3/ NS-EN 1991-1-4:2005+NA:2009. Eurocode 1: Action on structures. Part 1-4: General actions – Wind actions

/4/ N400 Bruprosjektering. Statens Vegvesen.

/5/ Vurdering og sammenlikning av brukonsepter for kryssing av Bjørnafjorden. Oppetid. Versjon 1.0. 25.04.2016.

/6/ Theory of Bridge Aerodynamics. E.Strømmen. Springer. 2006.

7 Appendices

Mathcad sheet – Simplified dynamic wind calculation model

Mathcad Sheet – Full dynamic wind calculation model.

AAS-JAKOBSEN COWI Multiconsult

JOHS HOLT AkerSolutions entail NGI DISSING+WEITLING architecture a|s mossmaritime

Concept development, floating bridge E39 Bjørnafjorden

Appendix E – Enclosure 10

10205546-08-NOT-184

Aerodynamic stability of K12

MEMO

PROJECT	Concept development, floating bridge E39 Bjørnafjorden	DOCUMENT CODE	10205546-08-NOT-184
CLIENT	Statens vegvesen	ACCESSIBILITY	Restricted
SUBJECT	Aerodynamic stability of K12	PROJECT MANAGER	Svein Erik Jakobsen
TO	Statens vegvesen	PREPARED BY	Allan Larsen
COPY TO		RESPONSIBLE UNIT	AMC

SUMMARY

This memo summarises the wind stability of the bridge girders of the K12 alternative for Bjørnafjorden bridge.

The memo concludes that the bridge is aerodynamically stable at wind speeds up to and beyond the requirements set by Håndbok N400 Bruprosjektering.

0	15.08.2019	Final issue	A. Larsen	R. M. Larssen	S. E. Jakobsen
REV.	DATE	DESCRIPTION	PREPARED BY	CHECKED BY	APPROVED BY

Table of Contents

1 Wind load class

Following N400 /1/, section 5.4.3, a bridge shall be considered wind load class III when the following criteria apply:

- Highest eigen period > 2 s
- Span length > 300 m

Modal analyses of the K12 alternative for Bjørnafjorden floating bridge yields the highest eigen period to be 56.8 s. Further the main span of the cable stayed bridge is 380 m.

The above class III criteria are thus seen to be fulfilled. Hence verification of the wind stability of the bridge structure shall include interactions between the dynamics of the structure and wind field as well as aerodynamic stiffness and damping effects. The verification thus includes assessment of vortex induced vibrations /1/ section 5.4.3.7 and check of aerodynamic instabilities /1/ section 5.4.3.8.

2 Critical wind speed for onset of aerodynamic instabilities

Following N400 /1/, section 5.4.3 the critical wind speed for onset of aerodynamic instabilities shall be higher than 1.6 times the 500 year return period, 10 min mean wind speed at bridge girder level:

$$V_{crit}(z) > 1.6 \cdot V_m(z, T = 600\ s, R = 500\ year) \quad (1)$$

Following the MetOcean Design Basis /2/ the 50 year return period, 10 min mean wind speed at z = 10 m level is $V_m(z = 10\ m, T = 600\ s, R = 50\ year)$ = $V_{m,b}$ = 30.5 m/s.

Extrapolation to the level of the cable stayed bridge (z = 65 m) proceeds following (2):

$$V_m(z) = C_{prob} \cdot V_{m,b} \cdot k_T \cdot ln\left(\frac{z}{z_0}\right) \quad (2)$$

/2/ defines k_T = 0.17 and z_0 = 0.01 m for the Bjørnafjord site.

C_{prob} is a coefficient that transform 50 year return wind speeds to other return periods R /3/:

$$C_{prob} = \sqrt{\frac{1 - 0.2 \cdot ln\left(-ln\left(1 - \frac{1}{R}\right)\right)}{1 - 0.2 \cdot ln\left(-ln\left(1 - \frac{1}{50}\right)\right)}} \quad (3)$$

For $R = 500$ (3) yields C_{prob} = 1.122. Taking z = 65 m, (1), (2) yields $V_{crit}(65) >$ **81.7 m/s.**

3 Bridge girder aerodynamic properties

The present evaluation of the aerodynamic stability of the K12 bridge alternative is based on discrete vortex computations of steady state wind load coefficients and Aerodynamic Derivatives (flutter coefficients) for the K12 cross section, Figure 3.1.

The steady state wind load coefficients obtained in /4/ are reproduced in Table 3.1.

Aerodynamic derivatives calculated for the non-dimensional wind speed range 4 < V/fB < 30 are shown in Figure 3.2

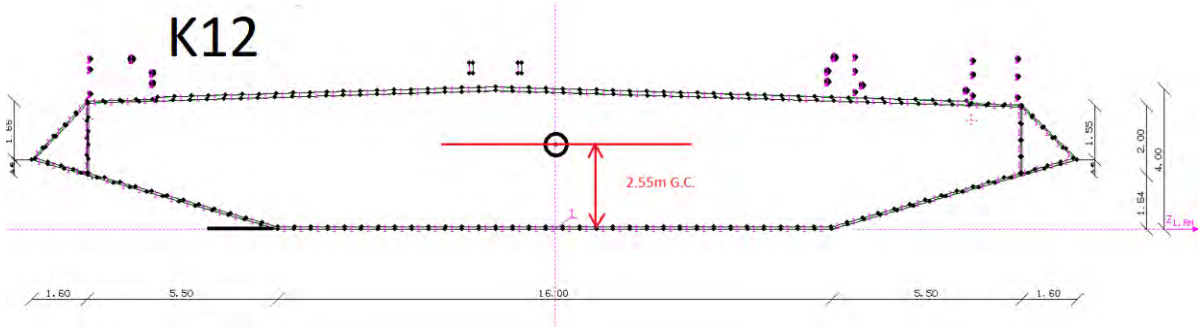

Figure 3.1 Discrete vortex panel model of the K12 cross section geometry.

Table 3.1 Steady state wind load coefficients for the K12 cross section from discrete vortex simulations.

C_{D0} [-]	C_{L0} [-]	$dC_L/d\alpha$ [$1/rad$]	C_{M0} [-]	$dC_M/d\alpha$ [$1/rad$]
0.675	-0.413	3.122	0.012	0.916

The wind load coefficients in Table 3.1 above are normalized the conventional way by the dynamic head of the wind $½\rho V^2$ and a characteristic dimension of the cross section. The section depth H = 4.0 m in case of the along wind drag loading and the cross section width B = 30.2 m in case of the lift and overturning moment.

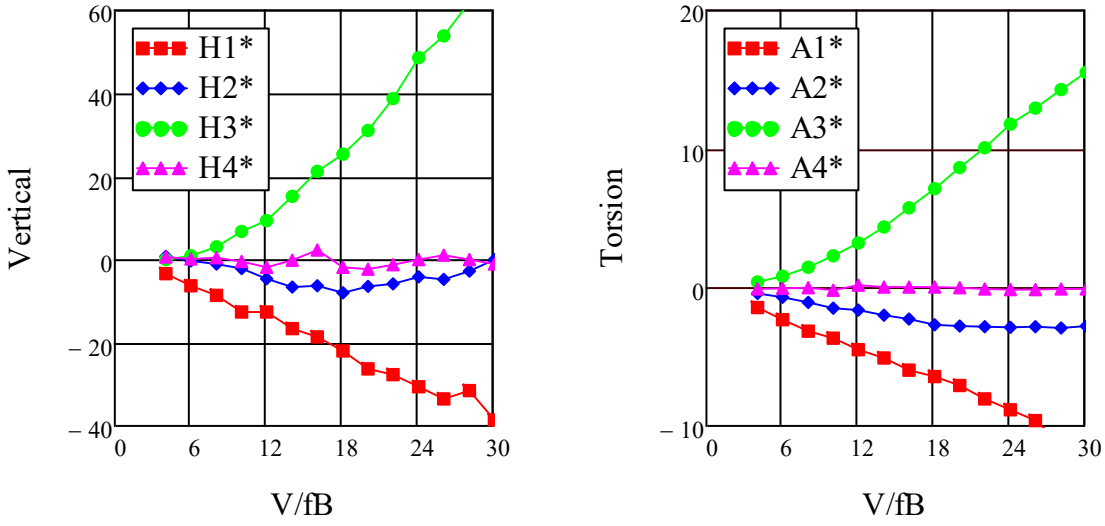

Figure 3.2 Aerodynamic derivatives for the K12 cross section from discrete vortex simulations.

The simulated aerodynamic derivatives shown in Figure 3.2 display the expected behaviour for non-dimensional wind speeds in the range $4 < V/fB < 18$ displaying a monotonic growth in a linear or parabolic fashion. For the highest non-dimensional wind speeds $18 < V/fB < 30$ it is noted that the $H_{2.4}^*$ and $A_{2.4}^*$ aerodynamic derivatives displays an unexpected non-monotonic behaviour which may influence stability calculations slightly.

4 Vortex induced vibrations

Vortex shedding in the wake of box girders may result in limited amplitude oscillations of the bridge girder at wind speeds where rhythmic vortex shedding locks on to a vertical bending or torsion eigen mode.

Practical experience from suspension bridges with shallow trapezoidal box girders have shown that vortex induced oscillations are usually confined to vertical modes only and occur at low wind speeds typically less than 12 m/s and for weather conditions with low atmospheric conditions.

Vortex induced vibrations of suspension bridges (Osterøy bridge, Norway and Storebælt East bridge, Denmark) has proven to be linked to severe flow separation and associated rhythmic vortex shedding at the knuckle line between the horizontal bottom plate and the lower inclined downwind side panel. Wind tunnel research /5/ has demonstrated that severe flow separation and vortex shedding can be avoided if the angle between the horizontal bottom plate and the lower side panels can be kept at approximately 15 deg. The 15 deg principle was recently introduced for the design of the girder of the Hålogaland Bridge, Norway and has proven to be free of vortex induced vibrations in full scale as well as in wind tunnel tests.

The design of the cross section shape of the girders of Bjørnafjorden bridge incorporates the 15 deg. principle. Thus, vortex induced vibrations are not expected to be an issue for the present design.

5 Verification of aerodynamic instabilities

N400 specifies that a wind load class III bridge shall be verified for four types of aerodynamic instabilities:

- Galloping
- Static divergence
- Classical flutter
- Torsion instability

Each type of aerodynamic instability will be discussed in separate sections below.

5.1 Galloping

Galloping is a cross wind vertical instability resulting in onset of vertical divergent oscillations above a certain threshold wind speed.

A necessary condition for galloping to occur is that the lift slope $dC_L/d\alpha$ is negative. With reference to Table 3.1 $dC_L/d\alpha$ = 3.122 > 0, thus galloping will not occur for the K12 design for Bjørnafjorden bridge.

5.2 Static divergence

Static divergence is a buckling type instability of the bridge girder occurring at the wind speed where the wind induced external moment acting on the girder exceeds the structural capacity. An estimate of the wind speed for onset for divergence V_{div} is given as /1/:

$$V_{div} = 2\pi f_\alpha \sqrt{\frac{2I_{\alpha eq}}{\rho B^4 \, dC_M/d\alpha}} \tag{4}$$

Where:

f_α is the eigenfrequency of the lowest torsion mode having modal mass M_α.

$I_{\alpha eq} = \frac{M_\alpha}{\int_0^L \varphi(x)^2 dx}$ is the corresponding equivalent mass moment of inertia.

ρ = 1.25 kg/m³ is air density

B = over-all girder width

The lowest torsion mode of the bridge is mode 11 displaying one partial half wave along the low level floating bridge, Figure 5.1, having an eigenfrequency f_α = 0.139 Hz and a modal mass M_α = 67.899·10^6 kg.

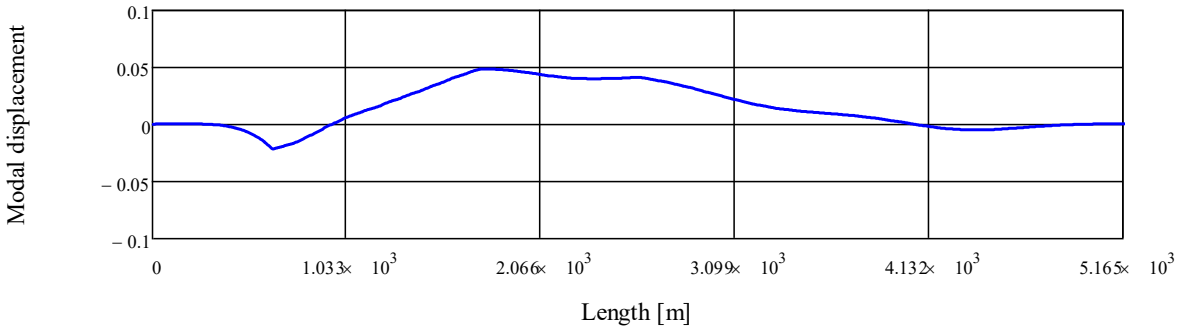

Figure 5.1 First torsion mode (mode 11) of Bjørnafjord K12 Alternative.

Inserting $dC_M/d\alpha$ = 0.916 and the above structural properties in (4) a divergence wind speed V_{div} = 174.9 m/s which is well above the requirement of 81.7 m/s.

5.3 Classical flutter

Classical flutter involves as a minimum two modes of motion. A torsion mode and a vertical bending mode of similar mode shape but with a lower eigenfrequency. The critical wind speed for onset of classical flutter is reached when the wind loading on the bridge girder makes the bending and torsion frequencies equal thereby establishing a resonant exchange of energy between to two modes. This in turn leads to divergent coupled torsion bending oscillations of the bridge girder. In cases where more vertical modes exist below the torsion mode these vertical modes may couple to form a compound vertical mode shape which couples with the torsion mode at the onset of flutter.

Different methods exist for calculation of the flutter wind speed of a bridge deck. The present method outlined in section 6 is an expansion of the AMC method (Air material Command) which allows an arbitrary number of modes and degrees of freedom of a bridge deck to couple into flutter /6/. The input to the flutter calculation constitutes the modes assumed to couple into flutter, the corresponding modal masses and eigenfrequencies and aerodynamic derivatives particular to the bridge deck.

The present multi-mode flutter analysis of Bjørnafjorden K12 alternative assumes that the first torsion mode and 9 vertical bending modes with lower vibration frequencies than the selected torsional mode may couple into flutter, Figure 5.2. Eigenfrequencies and modal masses with of the modes are listed in Table 5.1.

Table 5.1 Lowest vertical and torsion modal masses and eigenfrequencies. Bjørnafjord K12 alternative.

	Mode 15	**Mode 16**	**Mode 17**	**Mode 18**	**Mode 19**
Modal mass [kg]	16967 ·10^3	18696 ·10^3	28987·10^3	71188 ·10^3	43730 ·10^3
Eigenfrequency [Hz]	0.1449	0.1451	0.1543	01541	0.1536
	Mode 20	Mode 21	Mode 23	Mode 25	Mode 30
Modal mass	57772 ·10^3	52627 ·10^3	56610·10^3	91762 ·10^3	73227 ·10^3
Eigenfrequency [Hz]	0.1543	0.1546	0.1548	0.1550	0.1608

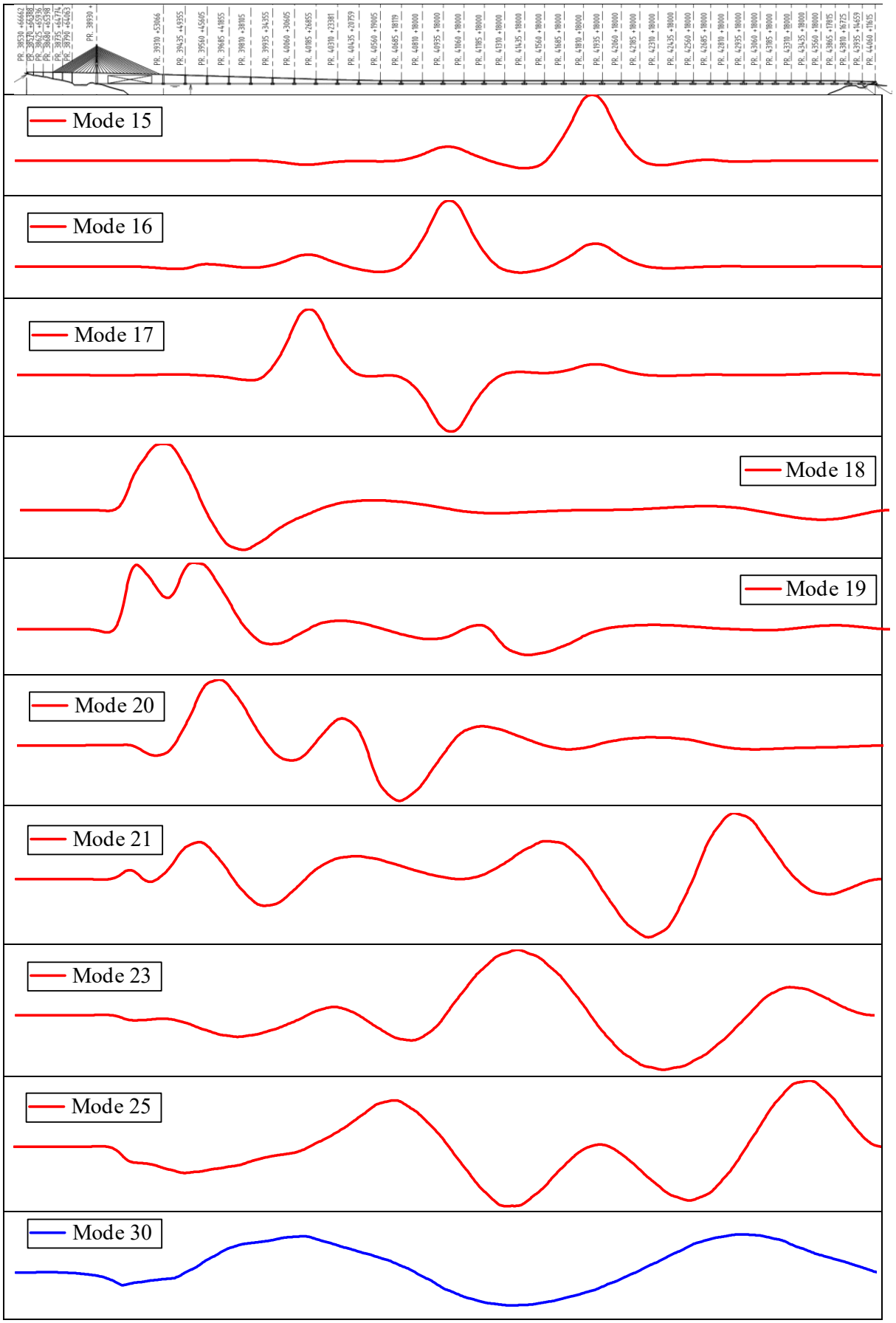

Figure 5.2 Flutter modes for Bjørnafjorden bridge K12 alternatives. Modes 15 – 25 (red) are vertical Mode 30 (blue) is torsion.

The mechanical damping of the bridge structure is an important parameter in flutter calculations as the requirement for onset of flutter is that the apparent aerodynamic damping exhausts the available mechanical damping. In the present context the mechanical damping available is obtained as the sum of the structural damping, the viscous damping, the hydrodynamic damping and the damping of the anchor lines. Aerodynamic damping is excluded as this component is included in the aerodynamic derivatives and varies as a function of wind speed.

The compound mechanical damping available in the bridge structure for the selected 10 modes are summarized in Table 5.2 from which it is noted that the lowest modal damping level is ζ = 0.0524 obtained for mode 18 which is assumed as a conservative lower bound for the flutter calculations.

Table 5.2 Compound mechanical damping computed for the selected flutter modes.

	Mode 15	**Mode 16**	**Mode 17**	**Mode 18**	**Mode 19**
Damping [rel-to-crit]	0.0955	0.0950	0.0937	0.0524	0.1184
	Mode 20	Mode 21	Mode 23	Mode 25	Mode 30
Damping [rel-to-crit]	0.0966	0.1147	0.1160	0.1033	0.1545

Flutter diagrams showing the outcome of the 10 mode analysis are shown in Figure 5.3. The apparent damping level to be balanced by the aerodynamics is $g = 2\zeta$ = 0.105, see section 6.

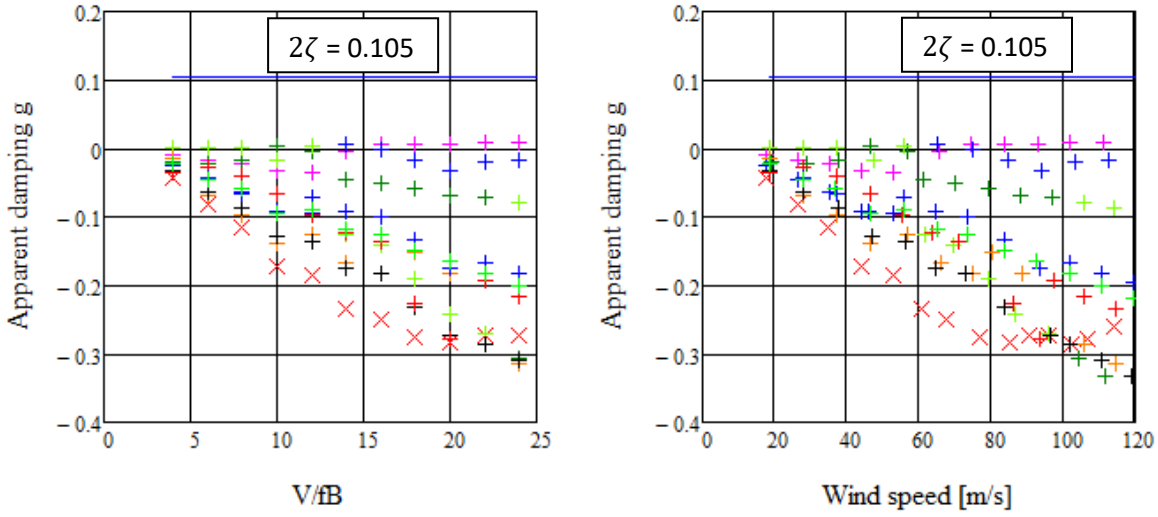

Figure 5.3 Apparent aerodynamic damping g as function of normalized and absolute wind speed for 2ζ = 0.105 Bjornafjorden K12 alternative.

From Figure 5.3 it is noted that all apparent damping levels remain below 2ζ = 0.105 for all wind speeds below 120 m/s. Hence the bridge is stable against classical flutter up to and beyond the N400 requirement of 81.7 m/s. It is noted that slightly positive apparent damping is found for wind speeds above V/fB > 10 or 45 m/s which indicates onset of flutter had the compound mechanical damping been below 0.003 (g = 0.006) as may be the case for land based suspension bridges.

5.4 Torsion instability

Torsion instability is a condition resulting in onset of torsional divergent oscillations above a certain threshold wind speed. Torsion instability is associated with the formation and travel of large coherent vortex structures across the bridge deck /6/. This type of instability is often associated with bluff plate girder bridge decks.

A necessary condition for the occurrence of torsion instability is that the A_2^* aerodynamic derivative change sign from negative at low wind speeds to positive at higher wind speeds.

From Figure 3.2 it is noted that A_2^* remains negative for all non-dimensional wind speeds up to at least V/fB = 30. It may thus be concluded that Bjørnafjorden K12 alternative will not encounter torsion instability at wind speeds below a wind speed of 30· $f_\alpha B$ = 125.9 m/s which is well above the N400 requirement.

6 Multimode flutter calculation

The calculation of the critical wind speed for onset of flutter follows from solving the complex valued eigenvalue problem (5) which combines the modal and aerodynamic properties of one torsion mode $\alpha(x)$ and n vertical bending modes $h1(x)$ … $hn(x)$, /6/.

$$Det\begin{bmatrix} 1+A_{\alpha\alpha}-\lambda_1 & \cdots & A_{\alpha hn} \\ \vdots & \ddots & \vdots \\ H_{hn\alpha}\left(\frac{f_\alpha}{f_{hn}}\right)^2 & \cdots & (1+H_{hnhn})\left(\frac{f_\alpha}{f_{hn}}\right)^2-\lambda_n \end{bmatrix}=0 \tag{5}$$

The individual elements in (5) combine modal and aerodynamic characteristics of the bridge deck girder and are composed as follows:

$$\begin{aligned} A_{\alpha\alpha} &= \frac{\rho B^4}{M_\alpha} C_{\alpha\alpha}(A_3^*+iA_2^*), & C_{\alpha\alpha} &= \int_0^L \alpha(x)^2 dx \\ A_{\alpha hn} &= \frac{\rho B^4}{M_\alpha} C_{\alpha hn}(A_4^*+iA_1^*), & C_{\alpha hn} &= \int_0^L \alpha(s)hn(x)dx \\ H_{hn\alpha} &= \frac{\rho B^2}{M_{hn}} C_{\alpha hn}(H_3^*+iH_2^*), & C_{hn\alpha} &= \int_0^L \alpha(s)hn(x)dx \\ H_{hnhn} &= \frac{\rho B^2}{M_{hn}} C_{hnhn}(H_4^*+iH_1^*), & C_{hnhn} &= \int_0^L hn(x)^2 dx \end{aligned} \tag{6}$$

The unknown to be solved for is the flutter frequency f which is embedded in the eigenvalues $\lambda_{n,j}$ through the identity:

$$Re(\lambda_{n,j}) + i\, Im(\lambda_{n,j}) = (1+ig_{n,j})\left(\frac{f_\alpha}{f}\right)^2 \tag{7}$$

Where $g_{n,j}$ is the apparent aerodynamic damping (negative) of a given mode at a given non-dimensional wind speed V/fB_j.

Once the complex eigenvalues $\lambda_{n,j}$ are determined for each of the non-dimensional wind speeds $V/fB_j = V_j^*$ for which the flutter derivatives are available, the equivalent aerodynamic damping and corresponding wind speed are obtained as:

$$g_{n,j} = \frac{Im(\lambda_{n,j})}{Re(\lambda_{n,j})}, \qquad V_j = V_j^* \frac{f_\alpha B}{\sqrt{Re(\lambda_{n,j})}} \tag{8}$$

By plotting the equivalent aerodynamic damping g as function of the wind speed the critical wind speed is identified where the sum of $g_{n,j}$ and twice the structural damping equals 0.

$$g_{n,j} + 2\zeta = 0 \tag{9}$$

6.1 Flutter calculation, Storebælt East bridge

The above flutter calculation procedure is illustrated in the example below which pairs the aerodynamic derivatives shown in Figure 3.2 with the structural properties of Storebælt East bridge section model (unity modes along the span) for which wind tunnel measurement of the critical wind speeds are reported in the literature /7/.

Storebælt East bridge section model structural data (two modes):

Mass / unit length: m = 22.74·10^3 kg/m

Mass moment of inertia / unit length: I = 2.47·10^6 kg/m

Vertical bending frequency: f_h = 0.1 Hz

Torsion frequency: f_α = 0.278 Hz

Deck width: B = 31 m

Structural damping: ζ = 0.003

Determination of the critical wind speed for onset of flutter following the above method is shown in Figure 6.1. It is noted that the red branch remains negative for all wind speeds. The purple branch starts being negative at low wind speeds but intersects the blue horizontal line (twice the structural damping) at a non-dimensional wind speed at V/fB = 12.4 (left diagram) corresponding to a critical wind speed of about 80 m/s (right diagram) which may be compared to a critical wind speed in the range 70 – 74 m/s measured in the wind tunnel /7/.

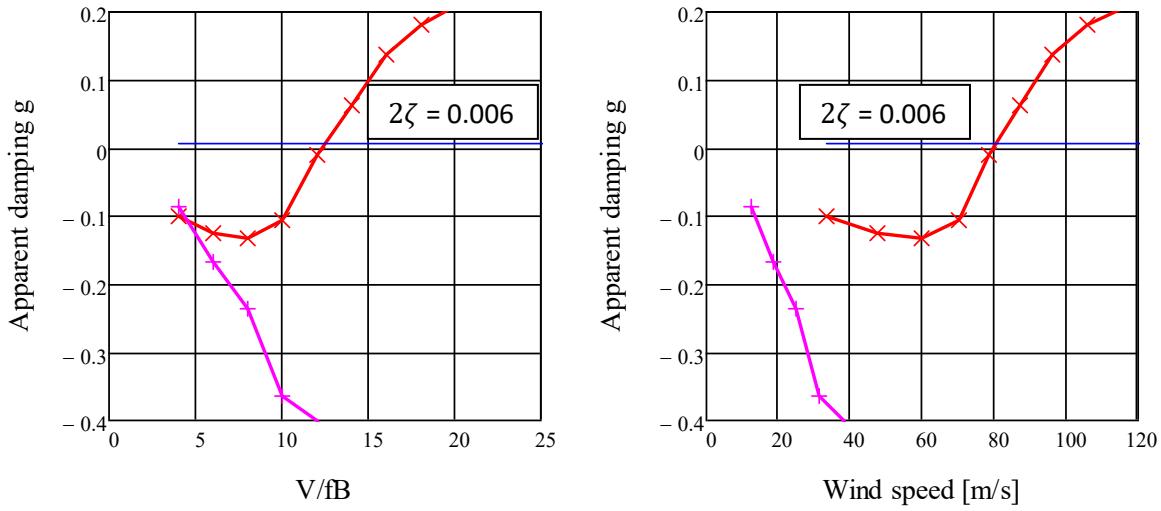

Figure 6.1 Determination of the critical wind speed for onset of flutter in non-dimensional for (left) and actual wind speed (right)

The geometry of the Storebælt East bridge and the K12 cross section is not identical, thus a perfect match of the flutter calculation applying the K12 aerodynamic derivatives to Storebælt dynamic data and the Storebælt wind tunnel tests cannot be expected. However, the relatively close match is quite satisfactory and supports the credibility of the computed aerodynamic derivatives for the K12 deck cross section.

7 References

/1/ N400: Håndbok, Bruprojektering, Statens vegvesen

/2/ MetOcean Design Basis. Document nr.: SBJ-01-C4-SVV-01-BA-001, 14-11-2018 including addendum of 18-03-2019.

/3/ Eurocode 1: Action on structures – Part 1-4: General actions – Wind actions. 2ed, 2007.

/4/ Memo 10205546-08-NOT-192 : CFD analysis of K12.

/5/ Larsen, A., Wall, A.: Shaping of bridge box girders to avoid vortex shedding response. Journal of Wind Engineering and Industrial Aerodynamics 104-106, (2012) 159-165.

/6/ Larsen, A.: Bridge Deck Flutter Analysis. Proceedings of the Danish Society for Structural Science and Engineering, Vol. 87, No. 2-4, 2016.

/7/ Larsen, A.: Aerodynamic aspects of the final design of the 1624 m suspension bridge across the Great Belt. Journal of Wind Engineering and Industrial Aerodynamics 48, (1993) 261-285.

Concept development, floating bridge E39 Bjørnafjorden

Appendix E – Enclosure 11

10205546-08-NOT-191

Cable vibrations of cable stayed bridge – K12

MEMO

PROJECT	Concept development, floating bridge E39 Bjørnafjorden	DOCUMENT CODE	10205546-08-NOT-191
CLIENT	Statens vegvesen	ACCESSIBILITY	Restricted
SUBJECT	Cable vibrations of cable stayed bridge – K12	PROJECT MANAGER	Svein Erik Jakobsen
TO	Statens vegvesen	PREPARED BY	Allan Larsen
COPY TO		RESPONSIBLE UNIT	AMC

SUMMARY

This technical note evaluates the risk of wind related vibrations of the stay cables of the Bjørnafjorden high bridge. The evaluation includes the following aerodynamic instability phenomena: Dry galloping, ice / sleet galloping, rain / wind galloping, and vortex induced vibrations.

It is found that wind related vibrations can be controlled to acceptable levels if the stay cables are equipped with dampers having a damping capacity similar to known commercial damper units.

It is recommended to acquire appropriate aerodynamic data through wind tunnel testing for the chosen cable pipes as part of the detailed design of the bridge.

0	15.08.2019	Final issue	A. Larsen	R. M. Larssen	S. E. Jakobsen
REV.	DATE	DESCRIPTION	PREPARED BY	CHECKED BY	APPROVED BY

Table of Contents

1 Introduction

Cable-stayed bridges are known to be prone to stay cable vibrations excited by the wind often in combination with precipitation such as rain, snow or ice. Stay cable vibrations has been an active field of research for more than two decades. However, the field has not yet matured to produce rigorous engineering codes of practice for support of load and stability calculations. Hence, the following assessment of aerodynamic stability of the stay cables of Bjørnafjorden K12 high bridge is based on the authors expert knowledge and compilation of research data and prediction models / methods available in the literature.

2 Acceptance criteria

EN1991-1-4, /1/, specifies that galloping need not be examined in detail if the onset wind speed V_{CG} as a minimum exceeds the mean wind speed $V_m(z)$ at level z as follows:

$$V_{CG} > 1.25V_m(z) \tag{1.1}$$

which, for the girder level z = 62 m /2/ becomes V_{CG} > 54.3 m/s, /2/.

Following EN1991-1-4 vortex shedding excitation of cable stays need not be examined in detail if the critical wind speed for vortex shedding excitation of the n'th cable mode exceeds the mean wind speed $V_m(z)$ at level z as follows.

$$V_{crit,n} > 1.25V_m(z) \tag{1.2}$$

In case stay cable vibrations cannot be excluded for wind speeds lower than V_{CG} or $V_{crit,n}$ the maximum allowable amplitudes A_{max} are defined as follows /3/:

$$A_{max} = \frac{L}{1700} \tag{1.3}$$

where L is the over-all length of the individual stay cables.

3 High bridge and stay cable properties

The cable stayed bridge is a single tower structure having a main span of 380 m and back spans of 140 m, 55 m, 55 m. The suspended spans are supported by four fans of stays each composed of 18 edge anchored cable stays, Figure 3.1.

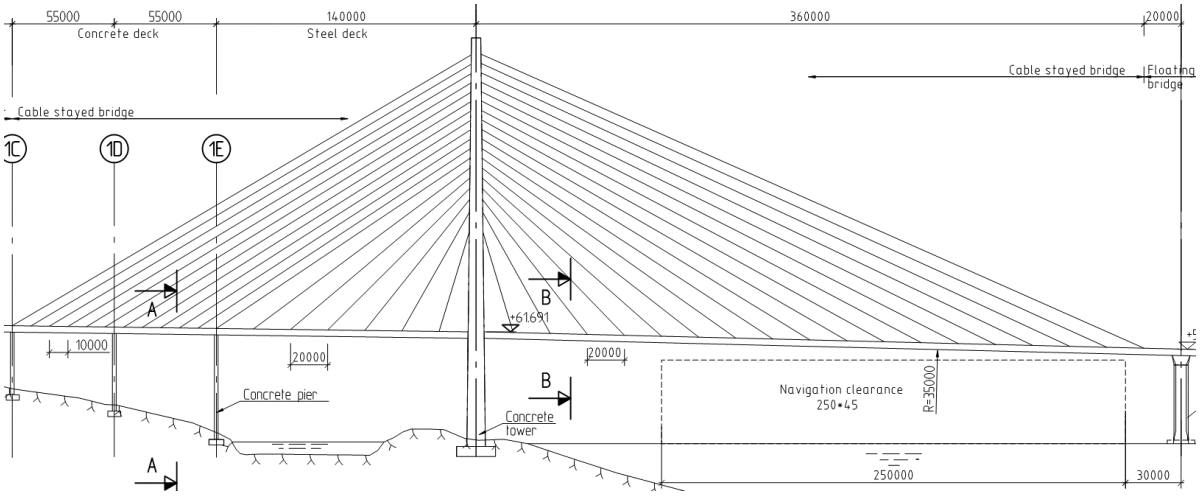

Figure 3.1 Bjørnafjorden high bridge, K12 alternative. Excerpt from drawing number SBJ-33-C5-AMC-22-DR-101.

The properties of the stay cables in the main and back spans relevant to the present assessment are summarized in Table 3.1, and Table 3.2.

*Table 3.1 Properties of the stay cables in the main span. Extracted from drawing number SBJ-33-C5-AMC-DR-105. Please note that *-marked diameters differs from final selected with up to 25mm. This has no practical implication on the conclusion in this note.*

Stay no	L [m]	S [m]	m [kg/m]	T [MN]	b [m]	θ [deg]	L_{ad} [m]
1	69	20	36.5	2.0	0.160	73.2	3.9
2	81	40	36.5	2.2	0.160	60.4	4.3
3	97	60	36.5	2.5	0.160	51.8	4.7
4	114	80	43.57	2.7	0.180	45.4	5.2
5	132	100	50.63	3.0	0.180*	40.7	5.7
6	150	120	50.63	3.2	0.200	36.9	6.2
7	170	140	64.76	3.4	0.200	34.6	6.5
8	189	160	64.76	3.6	0.200	32.2	6.9
9	209	180	64.76	3.8	0.200	30.5	7.3
10	229	200	64.76	4.1	0.200	33.1	7.6
11	249	220	71.83	4.4	0.200*	29.1	7.9
12	269	240	71.83	4.7	0.200*	27.9	8.2
13	289	260	71.83	4.9	0.225*	26.9	8.5
14	309	280	78.89	5.2	0.225*	25.9	8.7
15	329	300	78.89	5.2	0.225*	25.0	9.0
16	350	320	78.89	5.2	0.225*	24.2	9.1
17	370	340	78.89	5.2	0.225*	23.2	9.4
18	390	360	78.89	5.2	0.225*	22.6	9.6

Table 3.2 Properties of cable stays in the back spans. Extracted from drawing number SBJ-33-C5-AMC-DR-105

Stay no	L [m]	S [m]	m [kg/m]	T [MN]	b [m]	θ [deg]	L_{ad} [m]
1	69	20	36.5	2.0	0.160	73.2	4.6
2	81	40	36.5	2.2	0.160	60.4	5.1
3	97	60	36.5	2.5	0.160	51.8	5.6
4	114	80	43.57	2.7	0.180	45.4	6.2
5	132	100	43.57	3.0	0.180	40.7	6.7
6	150	120	50.63	3.1	0.200	36.9	6.7
7	170	140	50.63	3.3	0.200	34.6	7.3
8	181	150	50.63	3.5	0.200	34.0	7.8
9	192	160	64.76	3.6	0.200	33.6	8.0
10	203	170	64.76	3.8	0.200	33.1	8.0
11	214	180	64.76	4.0	0.200	32.7	8.1
12	225	190	64.76	4.2	0.200	32.4	8.2
13	236	200	71.83	4.1	0.225	32.1	8.3
14	247	210	71.83	4.5	0.225	31.8	8.4
15	258	220	71.83	4.6	0.225	31.5	8.4
16	270	230	71.83	4.8	0.225	31.6	8.4
17	281	240	71.83	4.9	0.225	31.3	8.5
18	292	250	71.83	5.0	0.225	31.1	8.5

where:

L is cable length [m]
S is horizontal distance from tower to anchorage [m]
m is linear cable mass [kg/m]
T is permanent load [MN]
b is diameter of HPDE cable tube

θ is cable angle with horizontal [deg]
L_{ad} is distance along cable from anchorage to damper unit [m]

The cable angle θ with horizontal is obtained as follows:

$$\theta = Acos\left(\frac{S}{L}\right) \tag{3.1}$$

The anchor to damper distance L_{ad} is inferred from the vertical anchor to damper distance measured off drawings SBJ-33-C5-AMC-22-DR-103, SBJ-33-C5-AMC-22-DR-104, assuming that all anchor tubes are to terminate at an equal height above the roadway.

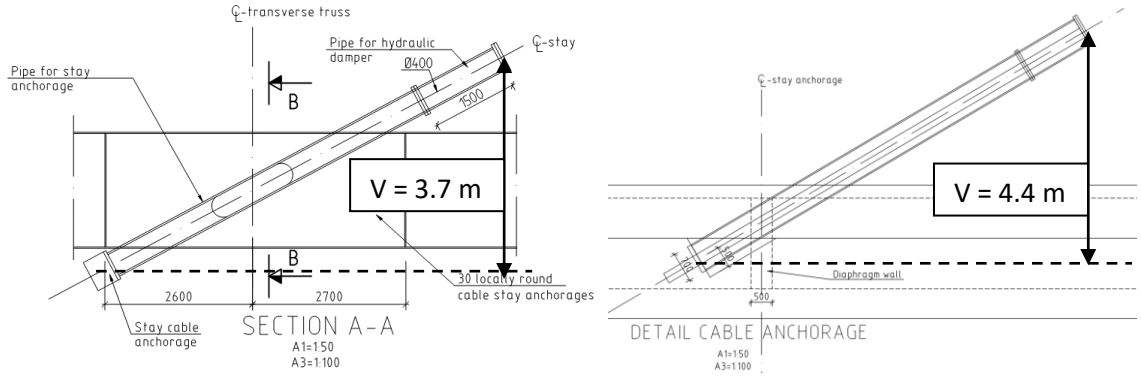

Figure 3.2 Say cable tubes for steel main span (left) and concrete back spans (right) indicating assumed vertical distances H between cable anchorage and damper location. Excerpt drawings SBJ-33-C5-AMC-22-DR-103, SBJ-33-C5-AMC-22-DR-104.

$$L_{ad} \approx \frac{V}{sin\left(Acos\left(\frac{S}{L}\right)\right)} \tag{3.2}$$

The first eigenfrequency f_1 corresponding to one ½-wave along the cable length is fundamental to stability considerations. f_1 for the main and back span stay cables are calculated following taut string theory (2.3) and displayed in Figure 3.3.

$$f_n = \frac{n}{2L}\sqrt{\frac{T}{m}}, \quad n = 1 \tag{3.3}$$

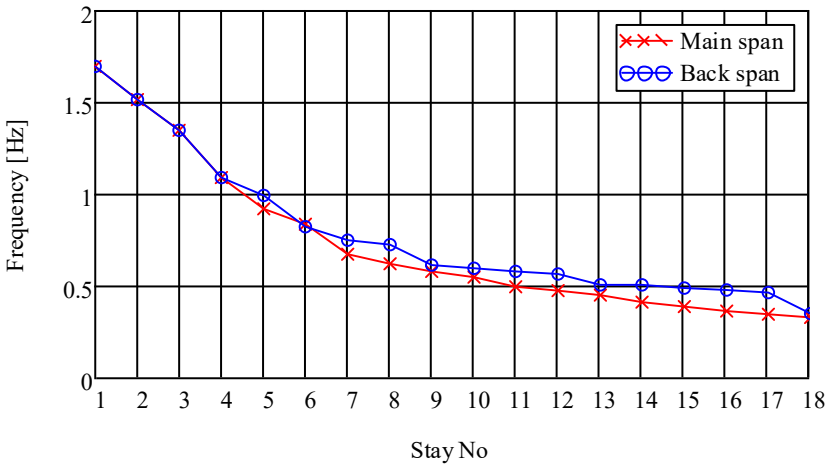

Figure 3.3 First mode eigenfrequencies f_1 (½-wave) of the main and back span stay cables of Bjørnefjorden high bridge.

It is noted that the first mode eigenfrequencies f_1 for the stay cables in the main and back spans falls in the range 1.7 Hz – 0.33 Hz with the longest stay cables having the lowest eigenfrequencies.

4 Stay cable dampers

It is common design procedure for cable stayed bridges to be fitted with cable dampers to prevent wind induced cable vibrations. A classical stay cable damper design is to arrange three hydraulic dashpot dampers (pistons) in a 120 degree star configuration as is exemplified by the Freyssinet commercial IRD damper, Figure 4.1.

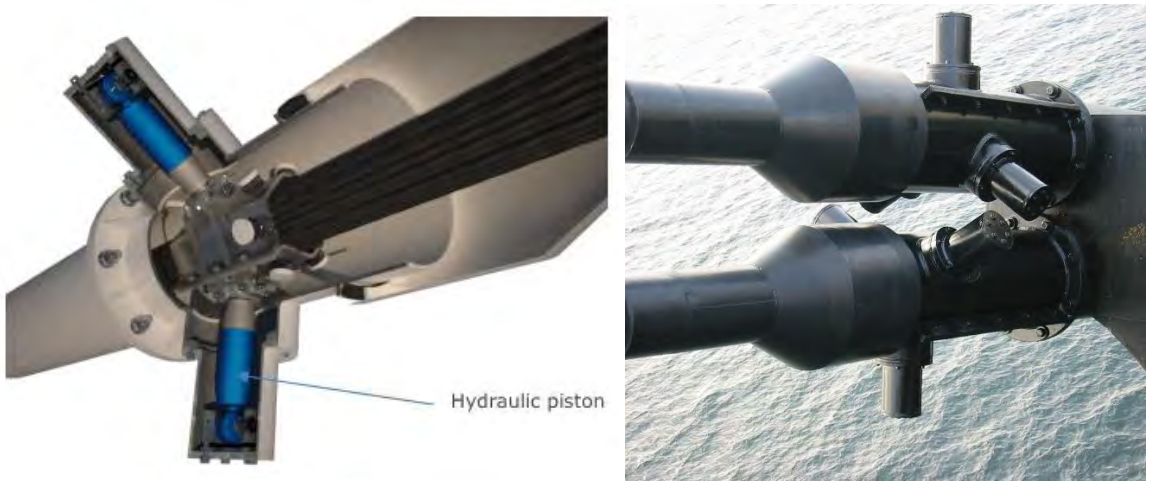

Figure 4.1 Hydraulic stay cable damper (Freyssinet IRD type). Cross section view (left). External view twin stay cables, Øresundsbron [right).

The compound damping coefficient of the IRD type damper depends on the performance of the individual dashpot units. However, available measurements (Øresundsbron) indicate a damping coefficient in the range 250 kNs/m < C < 300 kNs/m for practical installations. The present assessment assumes a damping coefficient C = 275 kNs/m.

The effective mechanical damping (rel.-to-crit.) of a stay cable vibrating in the first mode and fitted with a damper close to the anchorage can be estimated from equation (4.1) following /4/.

$$\zeta_m = \zeta_d + \zeta_s = \frac{L_{ad}}{L}\frac{\frac{2\pi L_{ad} C f_1}{T}}{1+\left(\frac{2\pi L_{ad} C f_1}{T}\right)^2} + \zeta_s \qquad (4.1)$$

where ζ_d represents the effect of the damper and ζ_s = 0.001 is the intrinsic structural damping of the stay cable /1/ (rel.-to-crit.). The resulting mechanical damping of the individual stay cable are shown in Figure 4.2, yielding expected damping levels in the range 0.011 – 0.016.

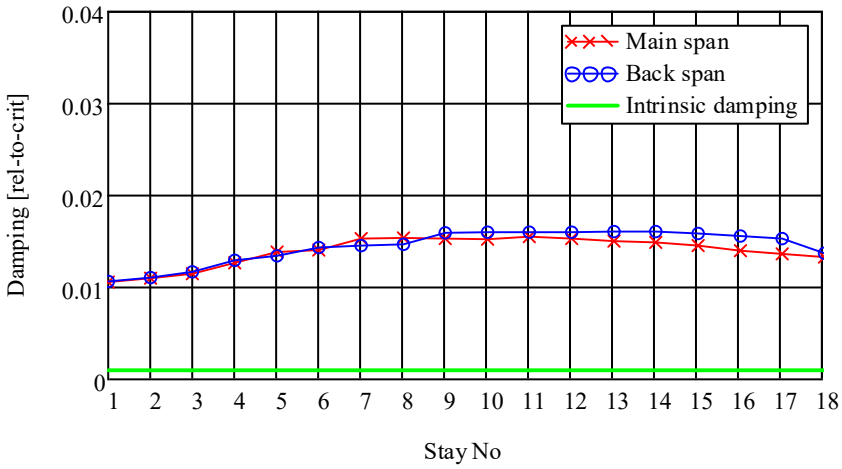

Figure 4.2 Estimated mechanical first mode damping of the main and back span stay cables.

5 Aerodynamic cable instabilities

The aerodynamic cable instabilities mentioned in the introduction (section 1) and their possible effects on the Bjørnafjord high bridge will be discussed and evaluated in the present section.

Known phenomena that may produce stay cable vibrations are as follows:

- Dry galloping – an instability associated with assymmetic flow separation on the cable cross sections. The asymetry may be caused either by the cable being in the critical Reynolds number range or by cable surface irregularities.
- Ice / sleet galloping – an instability associated with the deposit of ice, snow or sleet along the cabes causing the circular cable cross sections to be assymmetric to the wind.
- Rain / wind galloping – an instability associated with rain water draining along the cabes causing the circular cable cross sections to be assymmetric to the wind.
- Vortex induced vibrations – an instability associated with the alternating formation and shedding of vortices along the separtion lines at the upper and lower sides of the stay cable.

Common to the above instabilities are that they may be mitigated or delayed to higher wind speeds by introduction of additional mechanical damping to the stay cables.

Before venturing into the assessment a few concepts relating to the wind and stay cable geometry will be defined, Figure 5.1.

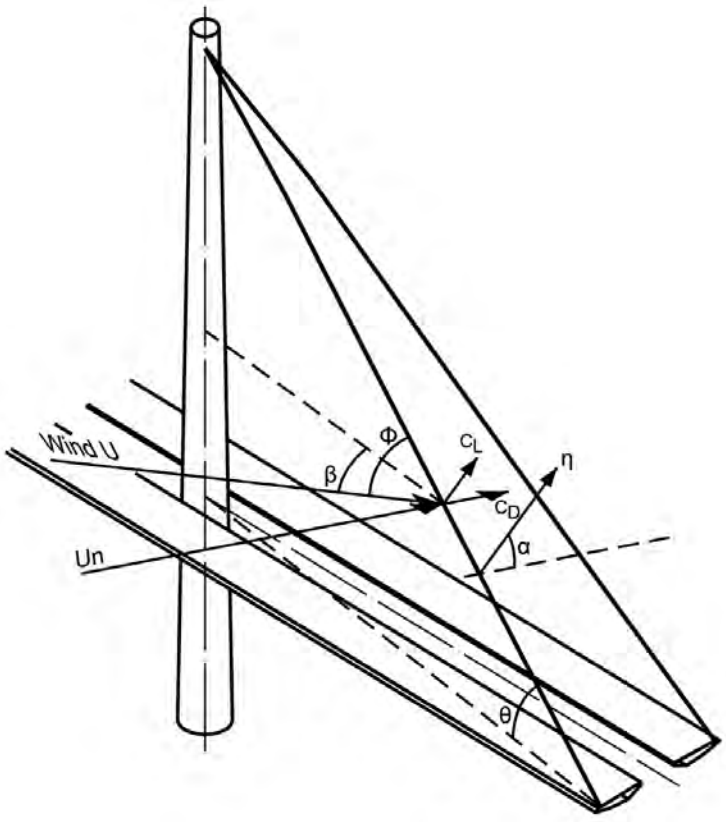

Figure 5.1 Definition of relations between the wind and the stay cables.

The angle ϕ between the wind direction and the direction of the stay cable known as wind-cable angle ϕ is found to be an important parameter for dry galloping. ϕ is related to the horizontal wind direction β and the cable angle relative to horizontal θ as follows:

$$cos\phi = cos\beta cos\theta \tag{5.1}$$

Thus, for a horizontal cable (θ = 0) $\phi = \beta$. For a vertical cable (θ = 90 deg.) ϕ = 90 deg.

5.1 Dry galloping

Dry galloping may occur as the wind flow about an inclined stay cable enters the critical Reynolds´ Number range ($2{\cdot}10^5 < Re < 3.5{\cdot}10^5$). I this range the drag coefficient C_D drops from a nominal value of 1.2 to approximately 0.4 while a distinctive cross-wind lift coefficient C_L may develop ($C_L \approx \mp 0.4$) due to asymmetric formation and location of the upper and lower separation lines along the cable.

The action of the Re dependent lift and drag forces produces a quasi-steady aerodynamic force in the direction of cable movements and thus a resulting negative aerodynamic damping which must be balanced by structural damping if cable movement is to be prevented.

The cable amplitudes due to dry galloping once started cannot be predicted. However, the critical wind speed and the damping necessary for prevention can be estimated from McDonalds aerodynamic damping function $Z(Re, \phi)$ which relies on experimental data (wind tunnel tests of inclined circular cylinders), Figure 5.2, /5/. Negative $Z(Re, \phi)$ values indicate positive aerodynamic damping adding to the structural damping. Positive $Z(Re, \phi)$ values indicate negative aerodynamic damping opposing the structural damping.

The criterion for stability against dry galloping is that the non-dimensional structural damping parameter Z_s is larger than $Z(Re, \phi)$:

$$Z_s = \frac{\zeta_m m f}{\nu \rho} > Z(Re, \phi) \tag{5.2}$$

where ν = $1.5{\cdot}10^{-5}$ kgm^{-1}/s is the kinematic viscosity and ρ = 1.25 kg/m^{-3} is the density of air.

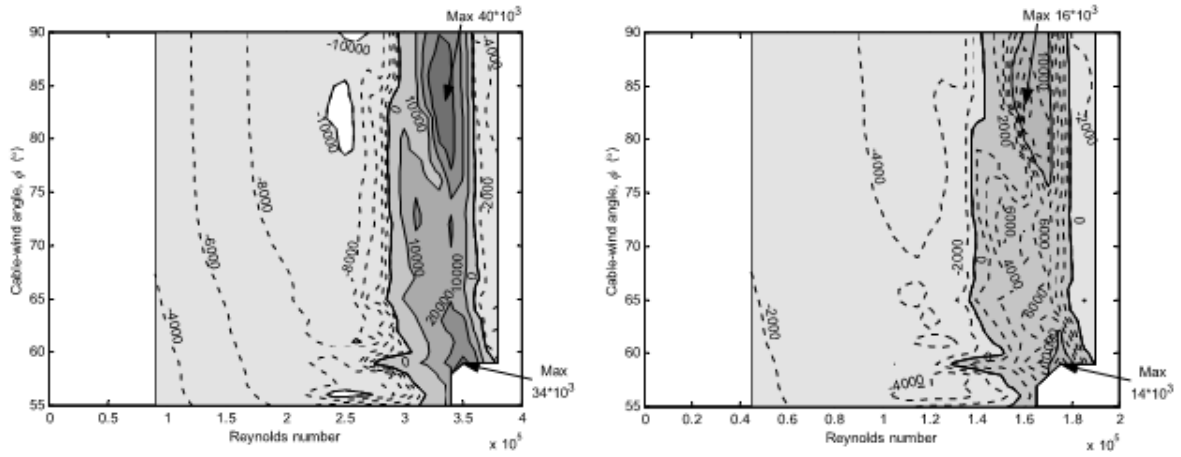

Figure 5.2 McDonalds aerodynamic damping function $Z(Re, \phi)$. Smooth flow (left). Corrected for the effects of 6% intensity turbulence (right).

The damping function shown in Figure 5.2, left is valid for smooth flow conditions for which the underling wind tunnel tests were carried out. Introducing turbulence has the effect of decreasing the Reynolds' Numbers for the critical range as well as making the transition in C_D from sub-critical to critical Reynolds' numbers more gradual. Correction of the smooth flow data according to ESDU /6/ to turbulent flow having 6% turbulence intensity typical of costal conditions yields reductions in the maximum damping and the corresponding Reynolds' Number, Figure 5.2, right.

From the left-hand graph (smooth flow) it is noted that maximum value of Z_{max} = $40{\cdot}10^3$ for Re_{max} = $3.3{\cdot}10^5$, where as the right-hand graph (turbulent flow) indicates a maximum value of Z_{max} = $16{\cdot}10^3$ for Re_{max} = $1.6{\cdot}10^5$. The corresponding wind-cable angle is ϕ_{max} = 83 deg.

With the aid of (5.1) the wind direction β relative to the cable planes for critical dry galloping conditions can be estimated for all cable stays Figure 5.3.

It is noted that critical conditions are expected for all cables in the interval 65 deg. < β < 82 deg. With the NE alignment of the bridge axis this coincides with the prevailing westerly winds at the bridge site.

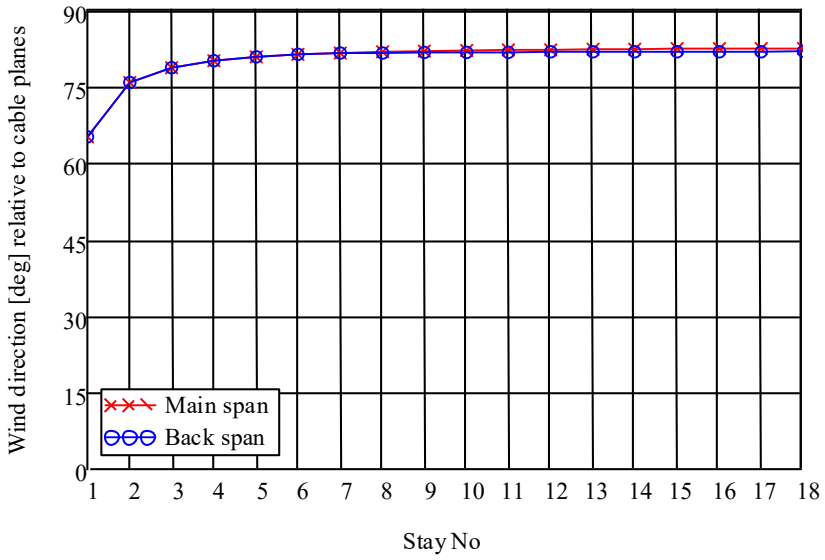

Figure 5.3 Wind direction β for maximum dry galloping excitation relative to the cable planes for the main and back span cable stays.

The critical wind speeds V_{CG} for dry galloping of the main and back span cables are calculated from the critical Reynolds' Numbers Re_{max} = 3.3·10^5, Re_{max} = 1.6·10^5 yielding maximum galloping excitation in smooth and turbulent flow:

$$V_{CG} = \frac{Re_{max}\nu}{b} \tag{5.3}$$

The estimated dry galloping wind speeds for the main and back span stay cables are shown in Figure 5.4 along with the EN1991-1-4 galloping criterion (1.1).

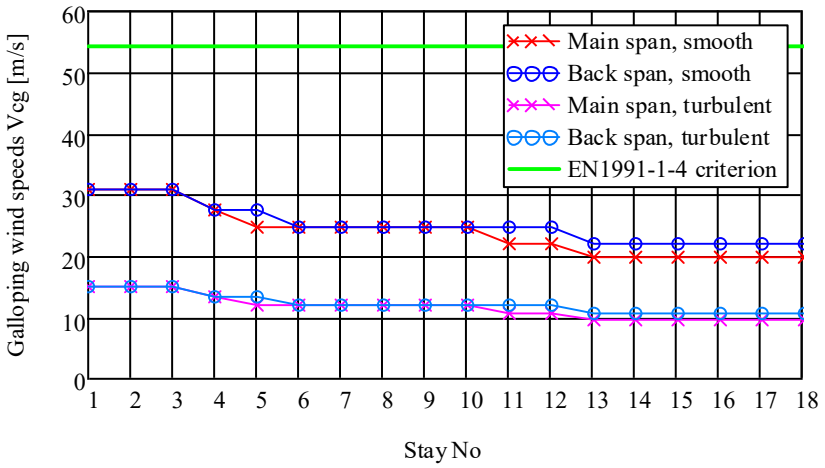

Figure 5.4 Calculated critical wind speeds for maximum dry galloping excitation of all cables in smooth flow.

From Figure 5.4 it is noted that the estimated dry galloping wind speeds for all stay cables falls below the EN1991-1-4 criterion demonstrating that cable dampers are necessary to prevent or delay the onset of dry galloping.

Calculated non-dimensional structural cable damping parameters Z_s according to eqn. (4.2) assuming intrinsic cable damping only (ζ_s = 0.001) and comparison to Z_{max} for smooth and turbulent flow are shown in Figure 5.6.

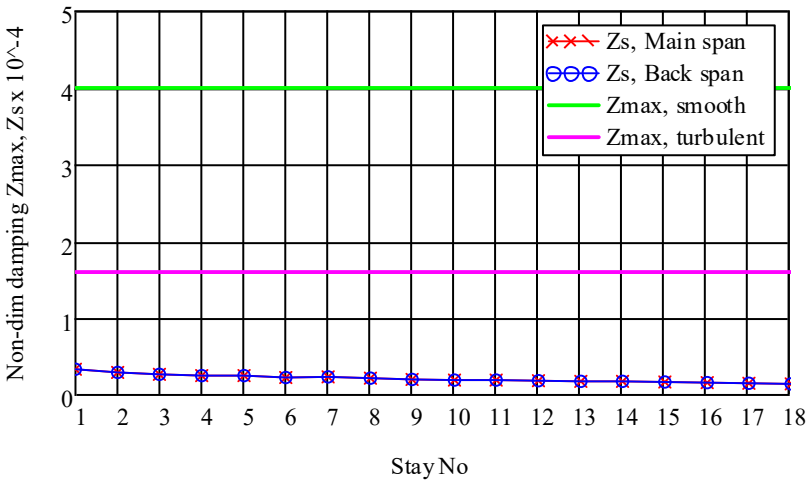

Figure 5.5 Calculated non-dimensional cable damping parameters and comparison to maximum smooth and turbulent flow values for the main and back span cable stays for intrinsic cable damping ζ_s = 0.001.

From Figure 5.5 it is noted that Z_s falls below Z_{max} for smooth flow as well as for turbulent flow conditions thus dry galloping is expected in case the stay cables are not equipped with cable dampers.

Inclusion of cable dampers will increase the mechanical damping substantially as shown in Figure 4.2, and will improve the dry galloping performance considerably as shown in Figure 5.6.

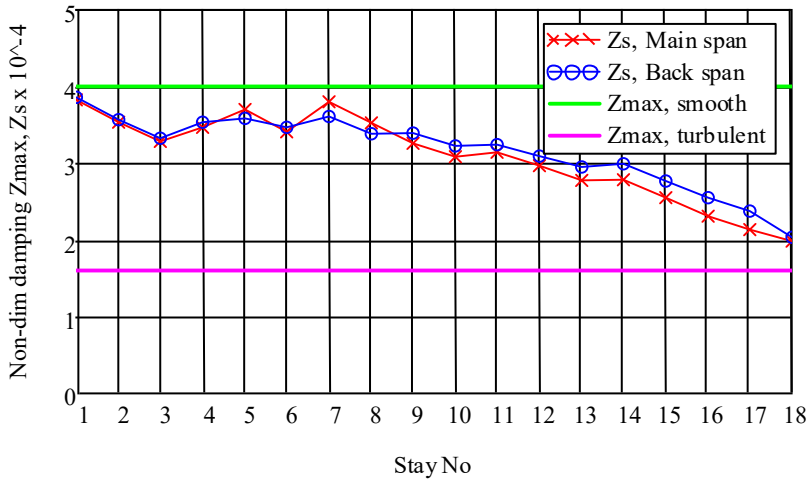

Figure 5.6 Calculated non-dimensional cable damping parameters and comparison to maximum smooth and turbulent flow values for the main and back span cable stays including damper units.

From Figure 5.6 it is noted that all stay cables are prone to dry galloping I smooth flow conditions with the structural damping parameter Z_s of the longest cables falling the most below the critical Z_{max} = 40·10^3 (green horizontal line). For turbulent flow conditions Z_s > Z_{max} = 16·10^3 for all stay cables. Hence dry galloping should not pose a problem if all stay cables are equipped with dampers having sufficient capacity.

5.2 Galloping due to cable surface irregularities

New research into the galloping of cylindrical cable surface elements has revealed that small deviations from the perfect circular cross section shape may cause substantial cross wind lift forces in the critical Reynolds number range $2 \cdot 10^5 < Re < 3.5 \cdot 10^5$. Wind tunnel measurements of the lift and drag coefficients as function of Re with the inflow angle α as parameter for a commercial HDPE tube having a diameter of 160 mm with $\pm$ 1 mm deviations, /7/, is reproduced in Figure 5.7.

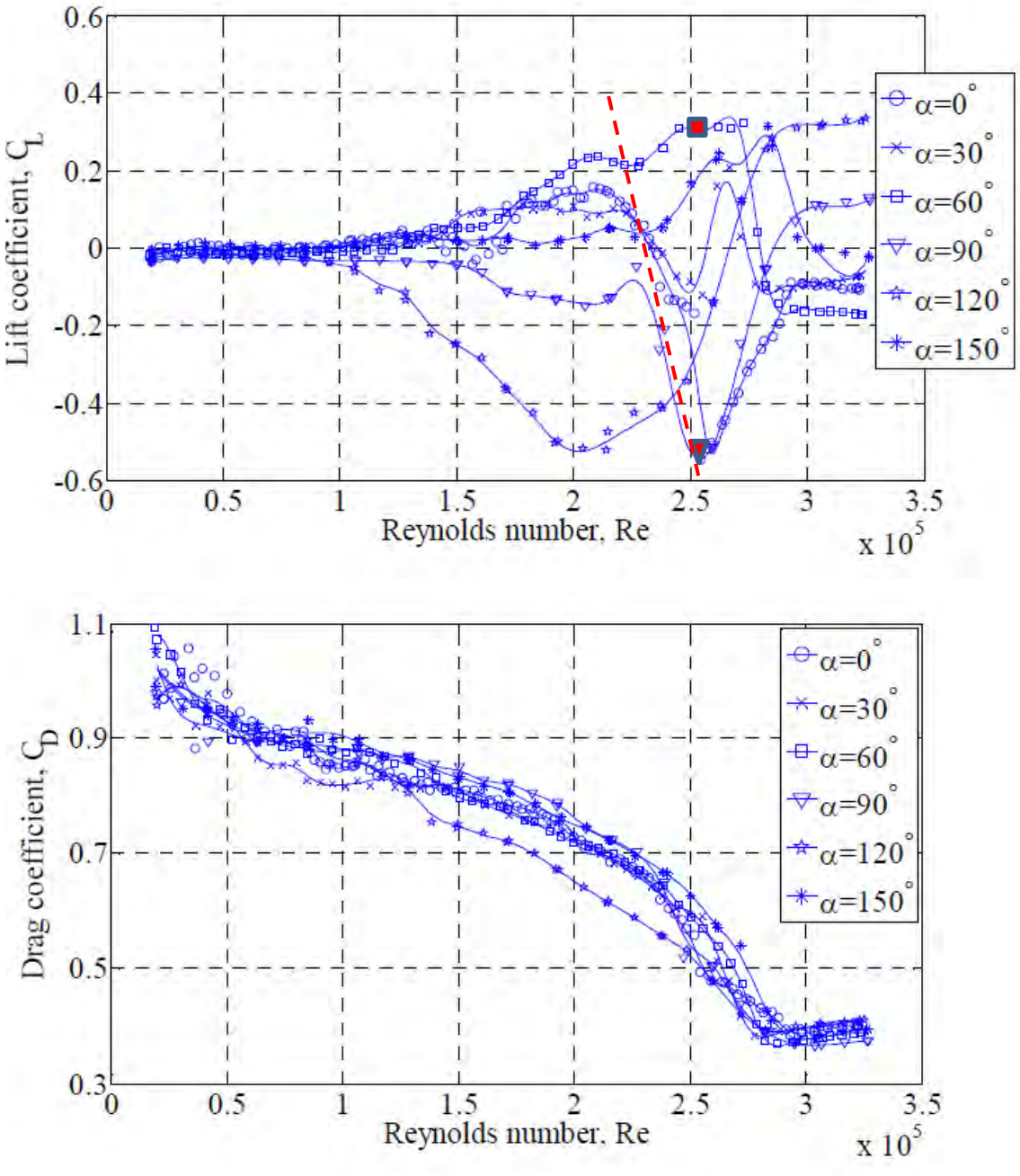

Figure 5.7 Variations of lift (upper) and drag (lower) coefficients as function of Re and inflow angle α for a commercial stay cable HPDE tube. Reproduced from /8/.

The data in Figure 5.7 may be interpreted to result in galloping by two different mechanisms:

1. Classical den Hartog galloping due to a negative gradient of the lift coefficient as function of inflow angle.

2. Dry galloping due to a negative gradient of the lift coefficient as function of the Reynolds' Number.

For the den Hartog type galloping the stability parameter is estimated as $a_G \approx 1$ at $Re = 2.5 \cdot 10^5$ (section 5.2.1). For dry type galloping the McDonald aerodynamic damping parameter is estimated as $Z \approx 2.72 \cdot 10^4$ (section 5.2.2).

Figure 5.8 demonstrates that the galloping wind speeds corresponding to $Re = 2.5 \cdot 10^5$ for onset of galloping due to surface defects will fall below the EN1991-1-4 criterion. Thus, cable dampers should be included to keep the aerodynamic damping sufficiently high to avoid galloping excitation.

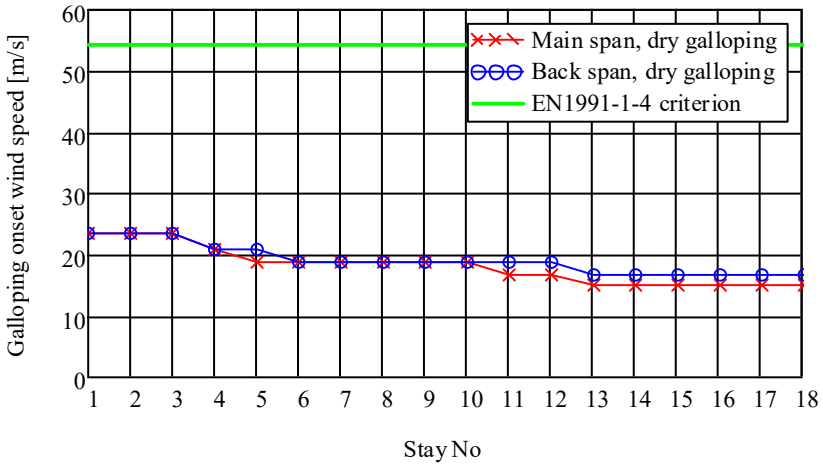

Figure 5.8 Evaluation of wind speeds for onset of dry galloping due to surface imperfections for all cable stays including cable dampers and comparison to the EN1991-1-4 galloping criterion.

The estimated non-dimensional damping parameter needed to damp aerodynamic excitation arising from surface imperfections (5.9) is illustrated in Figure 5.9. It is noted that $Z_S > Z = 2.27 \cdot 10^4$ stays 1 – 14, but slightly exceeded for stays 15 – 18. This may not seem satisfactory. However, it must be remembered, that Z calculated from (5.9) is likely to be conservative as the evaluation is based on a worst case estimate (one section of the cable and one inflow angle only). More elaborate evaluations based on wind tunnel tests dedicated to the actual cable HPDE pipes are expected to produce lower and more favorable Z estimates.

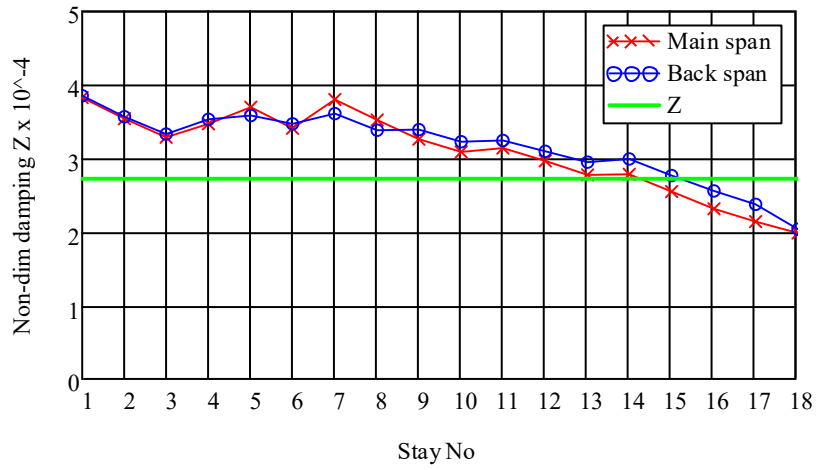

Figure 5.9 Calculated non-dimensional cable damping parameters for the main and back span cable stays including damper units and comparison to the aerodynamic non-dimensional damping estimated from (5.9).

5.2.1 den Hartog type galloping

From Figure 5.7 upper graph it is noted that the lift coefficient C_L at Re = 2.5· 10^5 varies substantially as function of the inflow angle α whereas the drag coefficient C_D displays relatively little variation. Estimation of the galloping stability parameter a_G at an inflow angle $\alpha \approx 75^0$ based on C_L, C_D data for $\alpha = 60^0$ ( ), $\alpha = 90^0$ ( ):

$$a_G \approx -\left[\frac{dC_L}{d\alpha} + C_D\right] = -\left[\frac{C_{L,90\ deg} - C_{L,60\ deg}}{90 - 60} \cdot 57.3 + C_D\right] = -\left[\frac{-0.5 - 0.3}{30} \cdot 57.3 + 0.55\right] \cong 1.0 \tag{5.4}$$

Following (5.4) galloping excitation due to cable surface irregularities may result in similar galloping excitation as ice accretion at critical Re (section 5.4).

Following EN1991-1-4 the wind speed for onset of den Hartog galloping can be estimated as:

$$V_{CG} = \frac{2Sc}{a_G} f_1 b = \frac{8\pi m_e f_1}{a_G \rho b} \tag{5.5}$$

where the effective mass m_e= m for sinusoidal cable mode shapes.

5.2.2 dry type galloping

Dry type (or Reynolds' Number dependent) galloping is governed by McDonalds damping function $Z(Re, \phi)$ which, for a circular cylindrical cable, may be expressed as /6/:

$$Z(Re, \phi) = \frac{Re}{16\pi}\left[-h(C_D) + \sqrt{g(C_D)^2 + g(C_L)^2 - h(C_L)^2}\right] \tag{5.6}$$

with auxiliary functions:

$$h(C_F) = g(C_F) + \frac{2C_F}{sin\phi}$$
$$g(C_F) = C_F\left(2sin\phi - \frac{1}{sin\phi}\right) + \frac{\partial C_F}{\partial \phi} cos\phi + \frac{\partial C_F}{\partial Re} Re \cdot sin\phi \tag{5.7}$$

with C_F = C_D or C_L.

Assuming $\phi \approx \phi_{max} \approx \pi/2$ and that the force coefficients C_D, C_L vary slowly as function of ϕ ($\partial C_F/\partial\phi \approx 0$) the auxiliary functions (5.7) can be simplified to read:

$$h(C_F) = 3C_F + \frac{\partial C_F}{\partial Re} Re \qquad g(C_F) = C_F + \frac{\partial C_F}{\partial Re} Re \tag{5.8}$$

which In turn yields the following approximate form of $Z(Re)$:

$$Z(Re) \approx \frac{Re}{16\pi}\left[-\left(3C_D + \frac{\partial C_D}{\partial Re} Re\right) + \sqrt{\left(C_D + \frac{\partial C_D}{\partial Re} Re\right)^2 - 4C_L\left(2C_L + \frac{\partial C_L}{\partial Re} Re\right)}\right] \tag{5.9}$$

With reference to Figure 5.7 it is noted that C_L exhibit strong negative gradients as function of Re for inflow angles α = 0^0 or α = 120^0.

Evaluation of the C_D, C_L gradients and Z for the Reynolds' Number range 2.4· 10^5 < Re < 2.6· 10^5 for α = 120^0 (following the red dashed tangent line in Figure 5.7) is outlined in Table 5.1.

In closing it should be noted that the evaluations in section 5.2.1 and 5.2.2 are based on pressure measurements made at one section along a commercial HPDE cable duct. Surface imperfections may vary along the span of the duct and lead to a pronounced span wise variation of C_D and C_L similar to the variation with inflow angle demonstrated in Figure 5.7. Such variations will decrease the tendencey for galloping or increase the onset wind speed.

Table 5.1 Evaluation of McDonalds aerodynamic damping function based on measured data, Figure 5.7, for inflow angle α = 120⁰.

$Re \cdot 10^5$	C_D	C_L	$\partial C_D/\partial Re$	$\partial C_L/\partial Re$	Z
2.4	0.8	-0.13	-	-	-
2.5	0.65	-0.22	$-1.75 \cdot 10^{-5}$	$-1.9 \cdot 10^{-5}$	$2.72 \cdot 10^4$
2.6	0.45	-0.51	-	-	-

5.3 Ice / sleet galloping

EN1991-1-4, Table E.7, proposes that galloping due to ice / sleet deposits is a similar process to classical den Hartog galloping and is caused by the change of the exterior cable surfaced due to ice accretion. For evaluation it may be represented by the stability parameter $a_G = 1$. However, contrary to dry galloping discussed in the previous section the aerodynamic force coefficients and thus a_G are assumed to independent of wind speed and thus also of the Reynolds' Number.

The aerodynamic damping (rel.-to-crit.) can be estimated from quasi steady assumptions as:

$$\zeta_a = \frac{\rho b V_m(z)}{4\pi m f_1} a_G \tag{5.10}$$

Which also may be expressed similarly to McDonalds aerodynamic damping function as:

$$Z = \frac{b V_m(z)}{4\pi \nu} a_G \tag{5.11}$$

As in the case of dry galloping a cable will be stable with respect to ice / sleet galloping in case $Z_s > Z$ (5.2), as is evaluated in Figure 5.10. It is noted that all stays are stable against ice / sleet galloping for wind speeds up to 15 m/s. At 20 m/s cable nos. 16, 17 and 18 are prone to galloping ($Z_s < Z$).

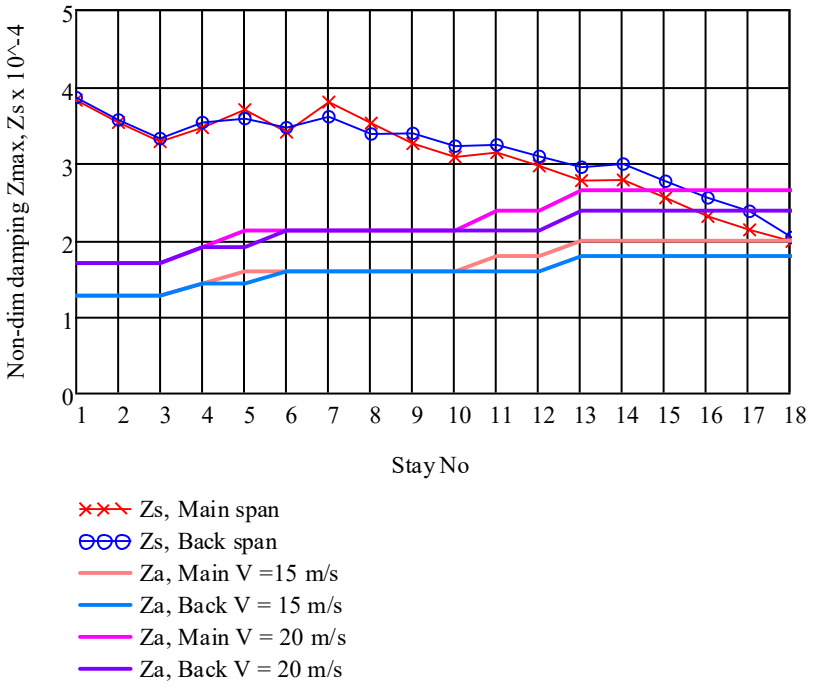

Figure 5.10 Calculated non-dimensional structural cable damping parameters Z_s and aerodynamic damping parameters Z corresponding to ice / sleet galloping at wind speeds 15 m/s and 20 m/s.

The evaluation presented in Figure 5.10 is only strictly valid for stay cables with ice accretions along the entre cable length. If ice accretion is restricted to a limited part of the cable the galloping excitation will be less and in part counterbalanced by positive aerodynamic damping along the parts of the cables free of ice / sleet.

It is possible to make allowance for the partial ice / sleet coverage assuming a limited extent of cable for which (5.10) applies, whereas the ice / sleet free parts receives aerodynamic damping associated with a circular cylinder in forced cross-wind oscillations. In this case (5.11) is modified to read:

$$Z = \frac{bV_m(z)}{4\pi\nu L}\left[a_G \int_{\frac{L}{2}-\Delta}^{\frac{L}{2}+\Delta} \varphi^2(x)dx - C_D \int_0^{\frac{L}{2}-\Delta} \varphi^2(x)dx\right] \tag{5.12}$$

where L is cable length, 2Δ is ice / sleet covered length about the cable midpoint and $\varphi(x)$ is the cable mode shape taken to be equal to ½ sine wave.

Figure 5.11 shows the development of Z as function of wind speed and the percentage of ice / sleet covered length compared to Z_s for stay cable no. 18 in the main span. It is noted that cable no. 18 is expected to stable up to wind speeds of about 15 m/s if completely covered by ice / sleet ($Z_s \geq Z$). If the ice coverage is reduced to about 50% the galloping wind speed is increased to 20 m/s. For ice / sleet covered lengths up to 22%, cable 18 is expected to be stable up to the EN1991-1-4 requirement of 54.3 m/s.

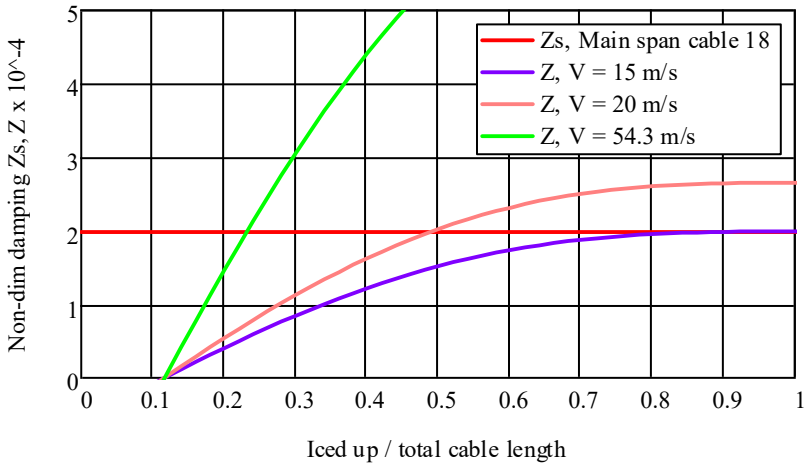

Figure 5.11 Non-dimensional damping parameters as function of wind speed and ice / sleet cover deposited symmetrically about the cable midpoint. Stay cable equipped with mechanical damper unit (section 4).

5.4 Rain / wind galloping

Based on observations made during the Erasmus Bridge cable vibration incident, Rotterdam, November 1994, /9/, the following model has been proposed for the maximum amplitude a of stay-cables (midpoint for 1 mode) excited by rain / wind:

$$a = \left(\frac{V_m(z)}{2\pi f_1}\right)\sqrt{\frac{8}{6\epsilon}}\sqrt{Y - \frac{8\pi f_1(\zeta_s + \zeta_d)}{\rho V_m(z) b}} \tag{5.13}$$

where:

ϵ = 8.0 is a non-linearity parameter

Y = 1.2 aerodynamic excitation [m]

ρ = 1.25 kgm^{-3} is air density

The parameters ϵ = 8.0, Y = 1.2 m assumed above are slightly conservative as compared to ϵ = 9.4, Y = 0.86 m originally derived for the Erasmus Bridge.

Evidence from incidents of rain / wind oscillations of stay-cables suggests that the oscillations tends to be strongest for wind speeds of about 15 m/s. Above this wind speed the water rivulet responsible for the cable oscillations tends to be blown off the cable surface thus stopping the excitation.

Plots showing the calculated maximum amplitudes for the main and back span cables with and without the proposed cable dampers are shown in graphical form in Figure 5.12, Figure 5.13 assuming a maximum wind speed of 15 m/s. The estimated amplitudes are compared to acceptance criterion $A_{max} < L/1700$ (1.3).

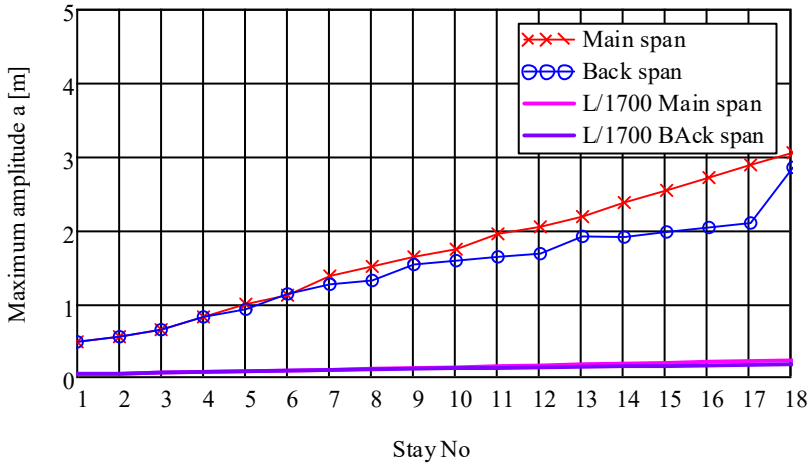

Figure 5.12 Predicted maximum (mid span) cable amplitudes due to rain / wind galloping at V = 15 m/s and comparison to criterion. Cables without dampers.

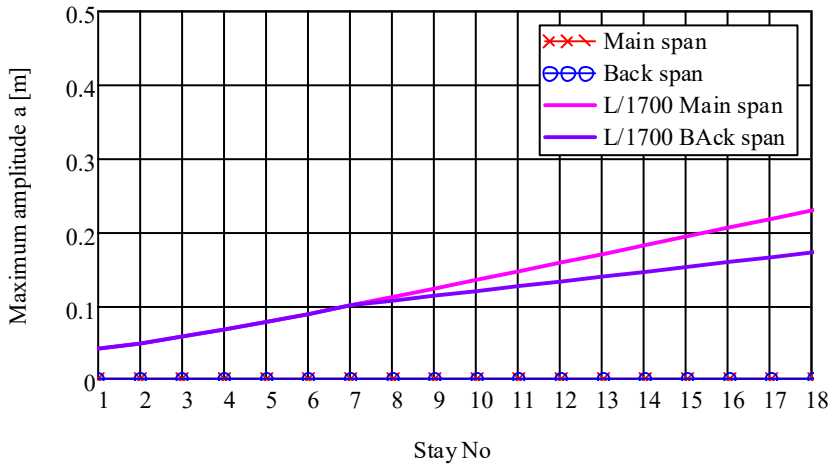

Figure 5.13 Predicted maximum (mid span) cable amplitudes due to rain / wind galloping at V = 15 m/s and comparison to criterion. Cables including dampers.

From Figure 5.12 it is noted that predicted maximum cable vibrations due to rain / wind galloping of the cables without dampers are expected to reach amplitudes in the range 0.5 m – 3.0 m thus exceeding the acceptance criterion. When including the mechanical dampers all cables are predicted to be stable against rain / wind galloping, $a \approx 0$.

6 Vortex shedding excitation

Vortex shedding excitation of a stay cable may occur when the frequency f_{vtx} of vortices shed in the wake of the cable coincides with one of the eigenfrequencies f_n (3.3) of the cable, $f_v = f_n$.

Following EN1991-1-4 the vortex shedding frequency is related to the wind speed and cable cross section diameter b through the Strouhal Number:

$$St = \frac{bf_v}{V} = 0.18 \tag{5.14}$$

Thus, the wind speeds for vortex induced vibrations of the stay cables is obtained as:

$$V_{crit,n} = \frac{bf_n}{St} = \frac{bf_n}{0.18} \tag{5.15}$$

Yielding the lowest critical wind speeds for the first modes of the stay cables (f_1), Figure 6.1.

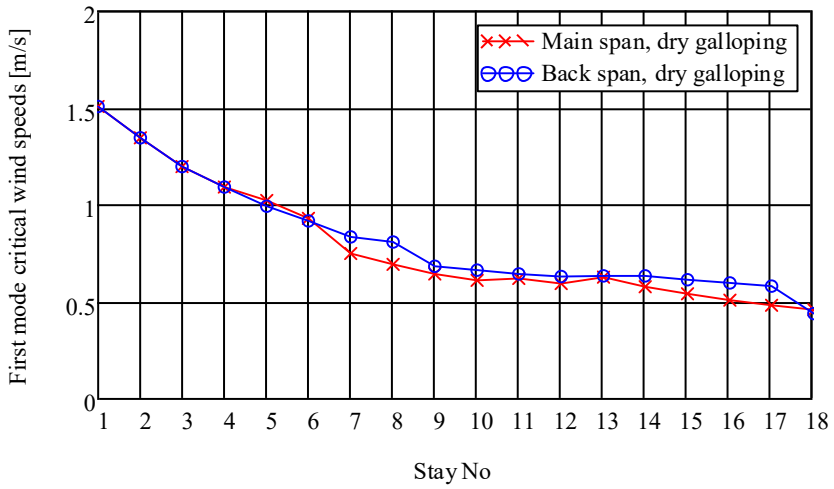

Figure 6.1 First mode critical wind speeds for vortex shedding excitation for all stay cables in main and back spans.

Figure 6.1 demonstrates that the first mode critical wind speeds fall in the range 0.5 m/s - 1.5 m/s thus $V_{crit,1}$ < 54.3 m/s following (1.2). The analysis then proceeds to evaluate expected amplitudes to be compare to (1.3).

For structures capable of responding in multiple modes (such as taut cables) EN1991-1-4 proposes the following expression (Method 1) for calculation of maximum amplitudes a due to vortex shedding excitation:

$$\frac{a}{b} = \frac{1}{St^2}\frac{1}{Sc}K \cdot K_w \cdot C_{lat} = \frac{1}{0.18^2}\frac{\rho b^2}{4\pi(\zeta_s + \zeta_d)}K \cdot K_w \cdot C_{lat} \tag{5.16}$$

with a recommended C_{lat} = 0.7 for Re < 2.5· 10^5 (sub-critical).

For sinusoidal mode shapes K= 0.101 and:

$$K_w = cos\left[\frac{\pi}{2}\left(1 - \frac{c_n bn}{L}\right)\right] \tag{5.17}$$

With the correlation length factor in the range 6 < c_n < 12 depending on the resulting amplitudes. For the present evaluation the more conservative value c_n= 12 is adopted. The resulting maximum amplitudes are shown in Figure 6.2, Figure 6.3 and compared to the acceptance criterion (1.3).

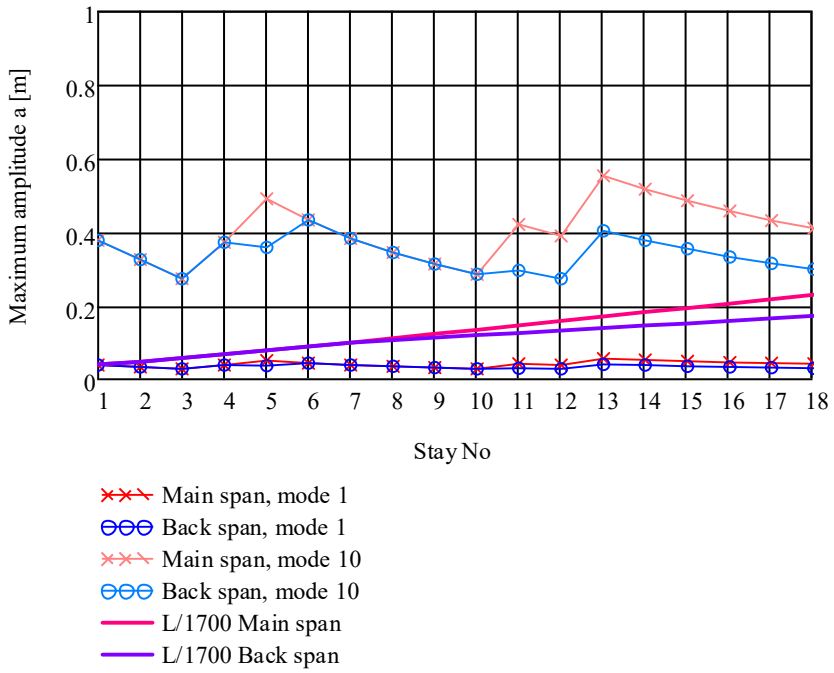

Figure 6.2 Maximum vortex induced amplitudes for 1`th and 10´th mode of the main and back span stay cables without dampers.

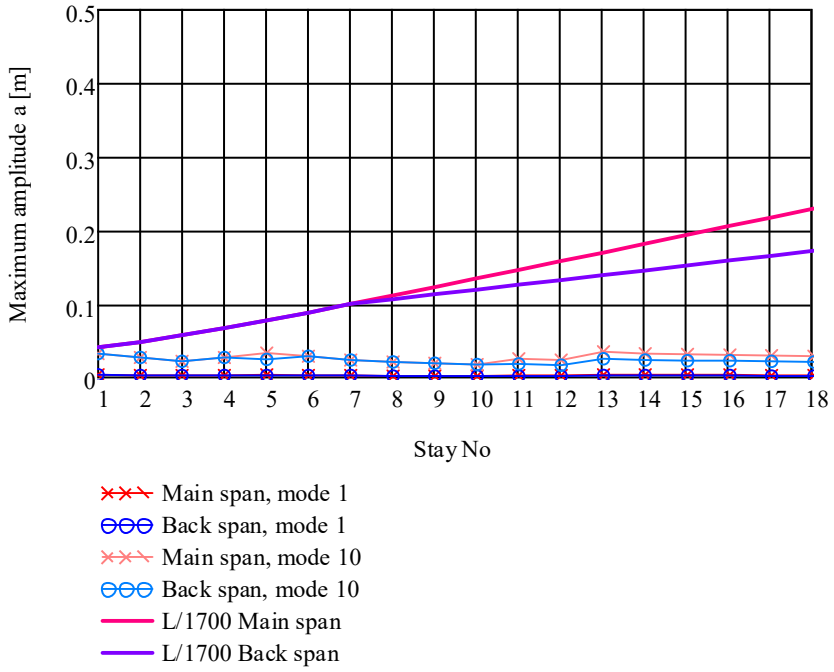

Figure 6.3 Maximum vortex induced amplitudes for 1`th and 10´th mode of the main and back span stay cables including dampers.

From Figure 6.2 it is noted that predicted 10'th mode amplitudes for the longer cable stay are exceeding the criterion in case the cables are not equipped with dampers. If the stay cables are equipped with dampers, Figure 6.3, all maximum amplitudes fall below the acceptance criterion.

7 Conclusion and recommendation

The present technical note has evaluated the risk of wind induced stay cable vibrations of the Bjørnafjorden high bridge.

It is found that the stay cables are likely to be free of unacceptable wind related vibrations in case they are equipped damper units having a damper capacity similar to currently available commercial designs. In case dampers are omitted, the stay cables are likely to receive unacceptable vibrations when exposed to winds above, say, 10 m/s at deck level.

The prediction models applied for the present assessment are based on data obtained for smooth surface stay cables and smooth cylinders. Contemporary HPDE pipe surface modifications such as helical fillets or dimples are not covered by the present analysis and may bias the outcome of the assessment. In view of this uncertainty it is recommended to verify the aerodynamic properties of the stay cable pipes by means of wind tunnel tests as part of the detailed design of the bridge.

8 References

/1/ Eurocode EN1991-1-4: Action on structures – Part 1-4: General actions – Wind actions. 2ed, 2007.

/2/ 10205546-08-NOT-184_0: Aerodynamic stability of K12, 15-08-2019.

/3/ Acceptance of stay cable systems using pre-stressing steels. *fib* Recommendation Bulletin 30:2005.

/4/ Krenk. S, Høgsberg, J. R.: *Damping of cables by a transverse force.* Journal of Engineering Mechanics, ASCE, April 2005.

/5/ McDonald, J. H. G.: Quasi-steady analysis of 2dof inclined cable galloping in the critical Reynolds´ Number range. Sixth International Symposium on Cable Dynamics, Charleston, SC, USA. 19-22 Sept. 2005.

/6/ ESDU, Item 80025C, 1986: Mean forces, pressures and flow field velocities for circular cylindrical structures: Single cylinder with two-dimensional flow.

/7/ Matteoni, G., Georgakis, C.T.: Effects of bridge cable surface roughness and cross-sectional distorsion on aerodynamic force coefficients. Proceedings, International Conference on Wind Engineering, ICWE13, 10-15 June 2011, Amsterdam, The Netherlands.

/8/ Guerts, C., Vrouwenvelder, T., Staalduinen, P. v.: Numerical modelling of rain-wind induced vibration. Erasmus Bridge, Rotterdam. SEI, Vol 8, Nr. 2, May 1998.

Concept development, floating bridge E39 Bjørnafjorden

Appendix E – Enclosure 12

10205546-08-NOT-192

CFD analysis of K12

MEMO

PROJECT	Concept development, floating bridge E39 Bjørnafjorden	DOCUMENT CODE	10205546-08-NOT-192
CLIENT	Statens vegvesen	ACCESSIBILITY	Restricted
SUBJECT	CFD analysis of K12	PROJECT MANAGER	Svein Erik Jakobsen
TO	Statens vegvesen	PREPARED BY	Mitja Papinutti
COPY TO		RESPONSIBLE UNIT	AMC

SUMMARY

This document presents a summary of aerodynamic values for the final design cross section K12. The numerical analysis was performed with the Computational Fluid Dynamics (CFD) tool to calculate the bridge deck aerodynamics. The Discrete Vortex Method (DVM) method inside commercial software package RM Bridge was used in these investigations. The CFD model is calibrated and compared to the wind tunnel tests from 3rd phase of BJF project. Details are available in the report *10205546-08-NOT-062 CFD Analysis of cross-sections*.

This memo presents results on K12 cross-section for both Quays-Steady State (QSS) and the unsteady flutter derivatives. A good match between the wind tunnel and numerically extracted results is observed, thus offers the required confidence level of the results. Provided validation also confirms the CFD extraction techniques. The aerodynamic performance of the selected cross section for the final design K12, and are compared to reference previous initial design cross section SS1.

0	15.08.2019	Final issue	M. Papinutti	R. M. Larssen	S. E. Jakobsen
REV.	DATE	DESCRIPTION	PREPARED BY	CHECKED BY	APPROVED BY

Table of Contents

1 About CFD

In RM Bridge, a CFD module is available for computing the aerodynamic coefficients C_D, C_L, C_M of different cross-sections. The plane airflow around the obstacle can be described by the two-dimensional Navier-Stokes equation. The assumption of incompressible fluids with constant viscosity is applied, resulting in the vorticity transport equations defined by:

$$\frac{\partial \omega}{\partial} + (\boldsymbol{u} \cdot \nabla)\omega = v\Delta\omega$$

Where

$\boldsymbol{u}$ = is the velocity of the fluid
ω = is the curl of this velocity (vorticity)
v = is the kinematical viscosity of air (0.000015 m^2/s at 20°C)

This equation is numerically solved for the open flow boundary conditions and deck wall assumption. The method used is the Discrete Vortex Method (DVM). The forces are calculated by the pressure integration of the two-dimensional cross-section, as a result of velocity filed around the deck depicted in Figure 1.

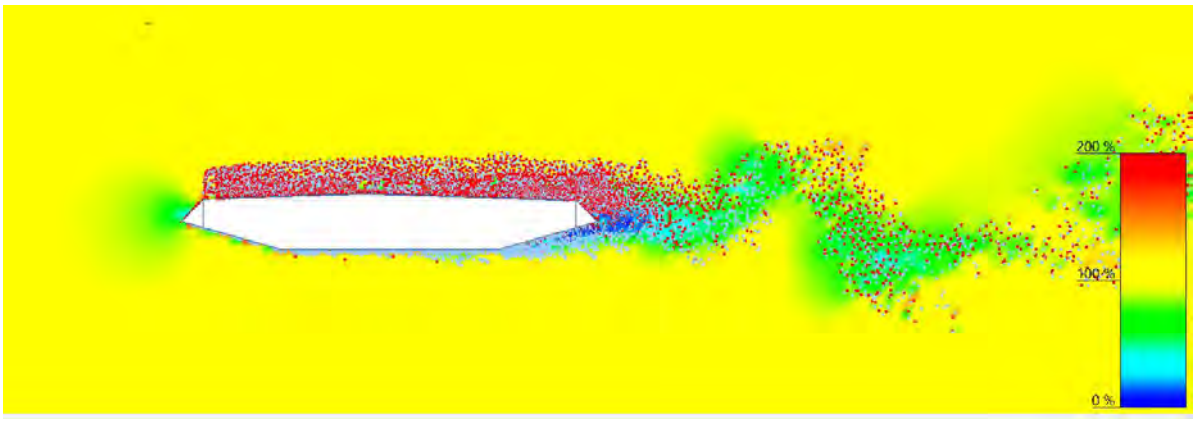

Figure 1: Velocity wind field around the deck and particle flow tracking, RM Bridge CFD tool.

2 Cross section geometry

The K12 cross section was modeled together with the 1.6m wide wind nose. The nose improves the aerodynamic performance introduction more controlled flow separation. The details of simplified fences and railings have were included in this investigation. The asphalt layer has been added to better simulated the top deck pressure redistribution. The cross-section dimension of K12 are depicted in Figure 2. The results are compared to the previous design cross-section SS1, depicted in Figure 3.

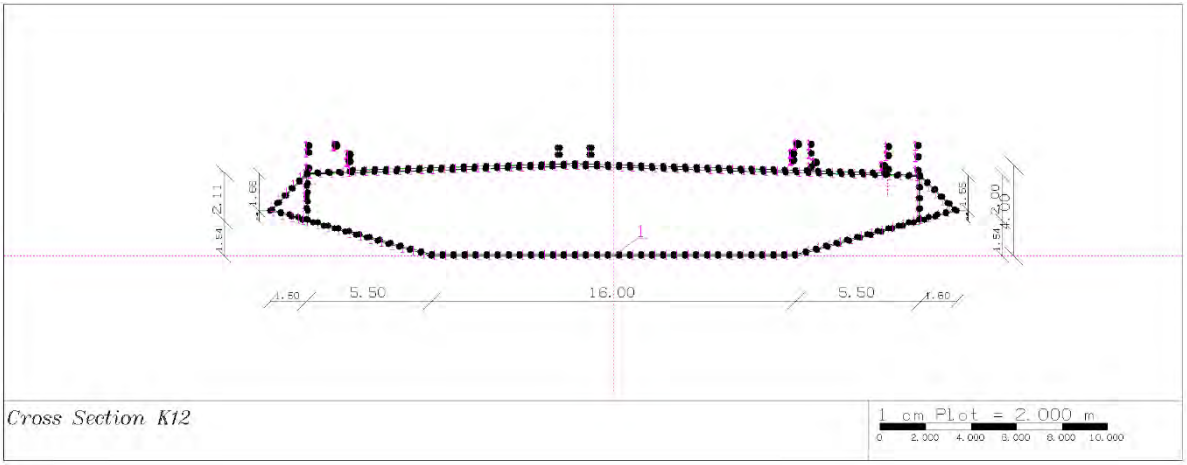

Figure 2: Finite element model of K12 cross section, used as final design cross section.

Figure 3: Finite element model of SS1 cross section, used for previous design cross section.

3 Quasi-steady state coefficients extraction

The Quasi-Steady State (QSS) aerodynamic forces is a mean value of fluctuating aerodynamic forces. They are commonly represented in a dimensionless format as:

$$C_D = \frac{1}{2}\rho V^2 H$$

$$C_L = \frac{1}{2}\rho V^2 B$$

$$C_M = \frac{1}{2}\rho V^2 B^2$$

Where for cross-section K12 following normalization are applied:

$$H = \ 4.0\,m \qquad (structural\ height)$$

$$B = 30.2\,m \qquad (width\ with\ the\ \text{wind nose})$$

The air density is assumed $\rho = 1.25\ kg/m^3$ and wind velocity is simulated for $V = 30\ m/s$. The CFD technique calculates the time-dependent forces for the drag, lift and moment direction. The time-dependent moment forces is presented in Figure 4. The mean value of QSS coefficient is calculated as the average of the time-dependent force, where 1/16 length of the signal is removed to avoid any transient effects.

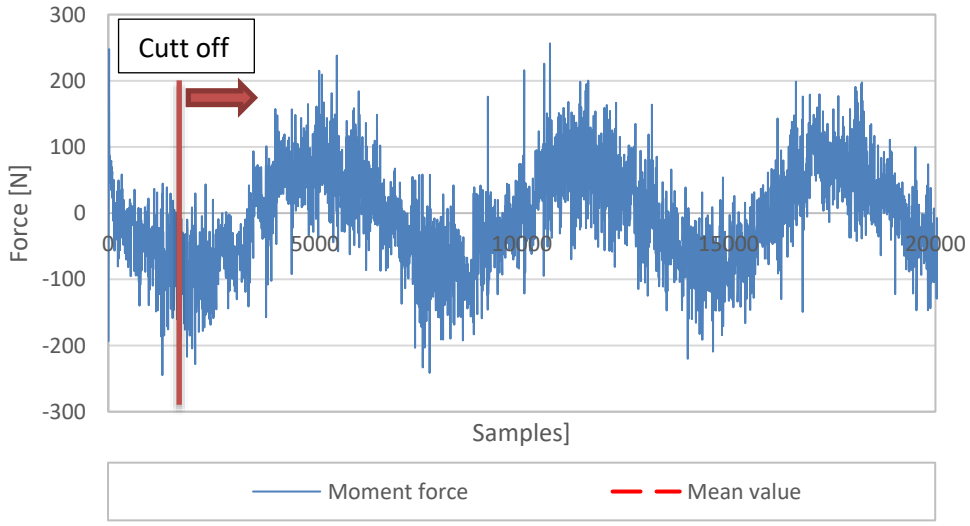

Figure 4: Time-dependent moment force and its mean value.

The aerodynamic coefficients for the final design cross section K12 is presented for the drag, lift and moment coefficients in Figure 5. The results are compared with the wind tunnel tests of similar shaped cross section K7 from a previous project phase. The main difference compared K7 to K12 are different wind shield, dimensions and fences details, both methods show a reasonable match in the results. Additionally, presented are results for SS1 cross section from a previous phase.

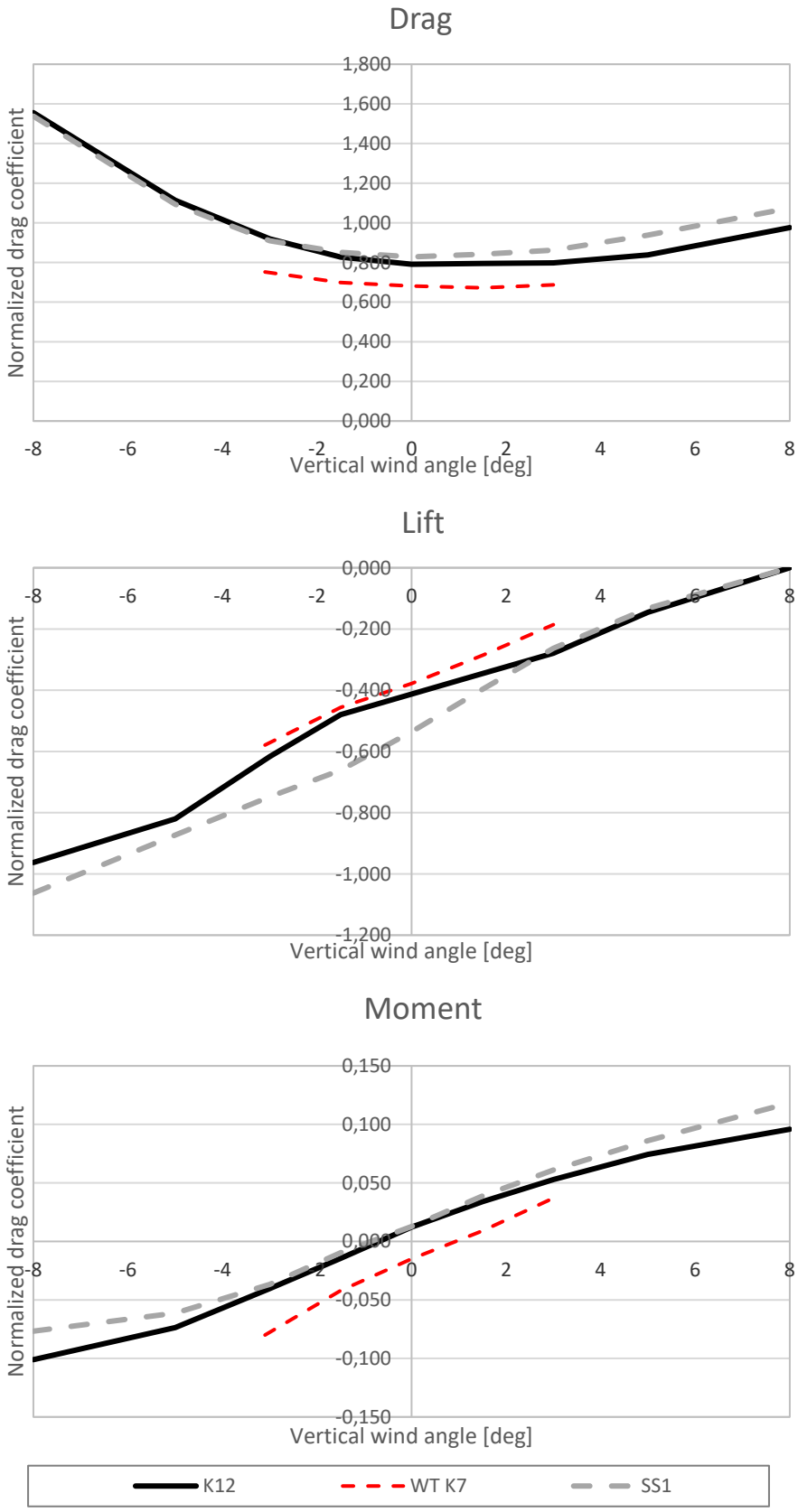

Figure 5 QSS coefficients for the Wind tunnel experiment on K7, previous design cross section SS1 and latest design cross section K12

4 Flutter derivatives

The Scanlan flutter derivatives are defined as motion dependent values. They are normalized values and are frequency dependent. For the two-dimensional aeroelastic cross-section following notation is commonly used for aeroelastic damping:

$$C_{se} = \frac{\rho B^2}{2}\omega \begin{bmatrix} H_1^* & BH_2^* \\ BA_1^* & B^2A_2^* \end{bmatrix}$$

and aeroelastic stiffness:

$$K_{se} = \frac{\rho B^2}{2}\omega^2 \begin{bmatrix} H_4^* & BH_3^* \\ BA_4^* & B^2A_3^* \end{bmatrix}$$

The flutter derivatives for vertical motion H_{1-4}^* and for pinch rotations A_{1-4}^* are expressed with dimensionless reduced velocity $\bar{V} = V/(B\omega)$ dependent functions. The presented formulation allows aerodynamically scalability form experiments to the real size structure. The coefficients extracted by CFD were conducted on a real size cross-section, thus eliminating any possible viscous flow effects, commonly present in the small-scaled wind tunnel tests. The extraction of rotation motion is presented in Figure 6.

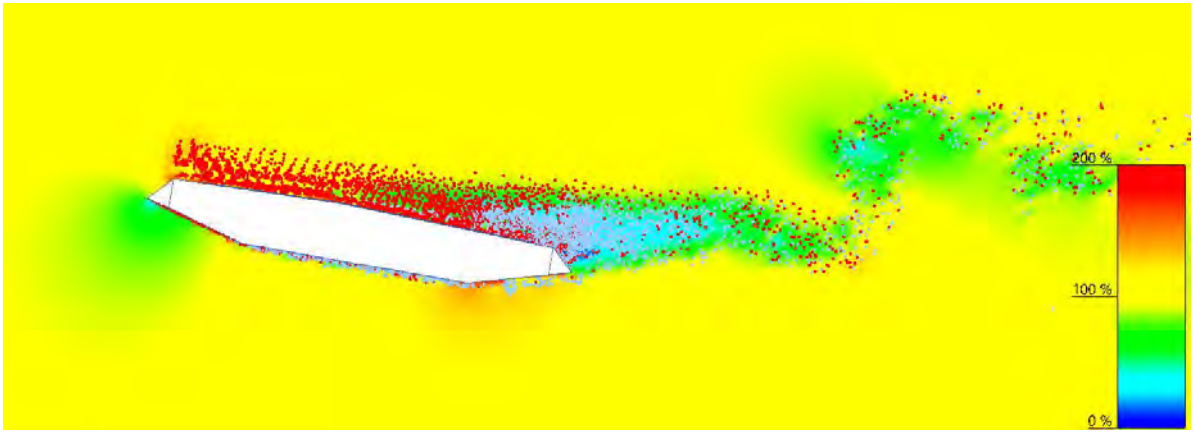

Figure 6: Flutter derivatives extraction simulation for amplitude 10° and 2 second motion rotational motion period

The flutter derivatives for the K12 cross section (black line) are presented for aeroelastic damping matrix in Figure 7 and aeroelastic stiffness in Figure 8. Results are compared with previous design cross section SS1. The reference values are compared to the similar Storebaelt cross-section shape. All three extracted flutter derivatives are showing similar trends and are typical for any closed aerodynamic deck section.

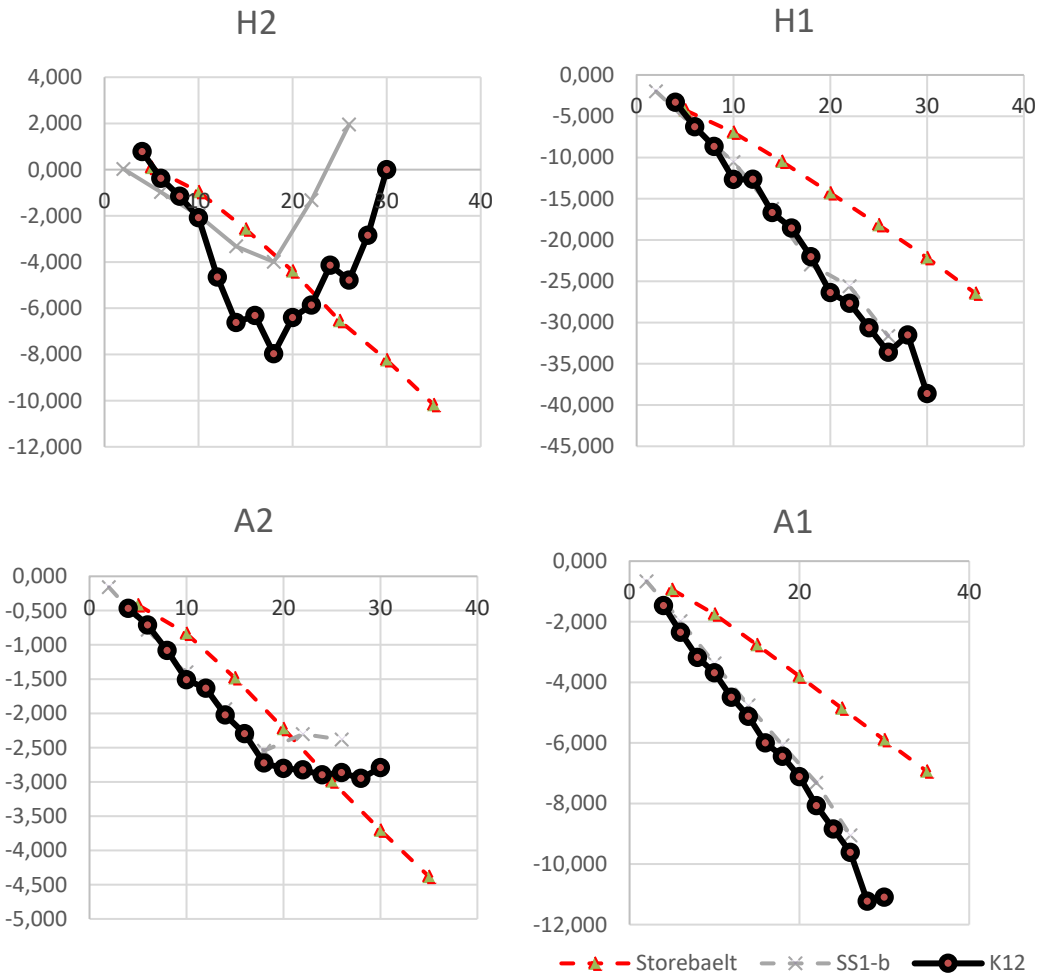

Figure 7 Aeroelastic damping flutter derivatives for; Storebaelt wind tunnel experiment, previous design cross section SS1 and latest design cross section K12

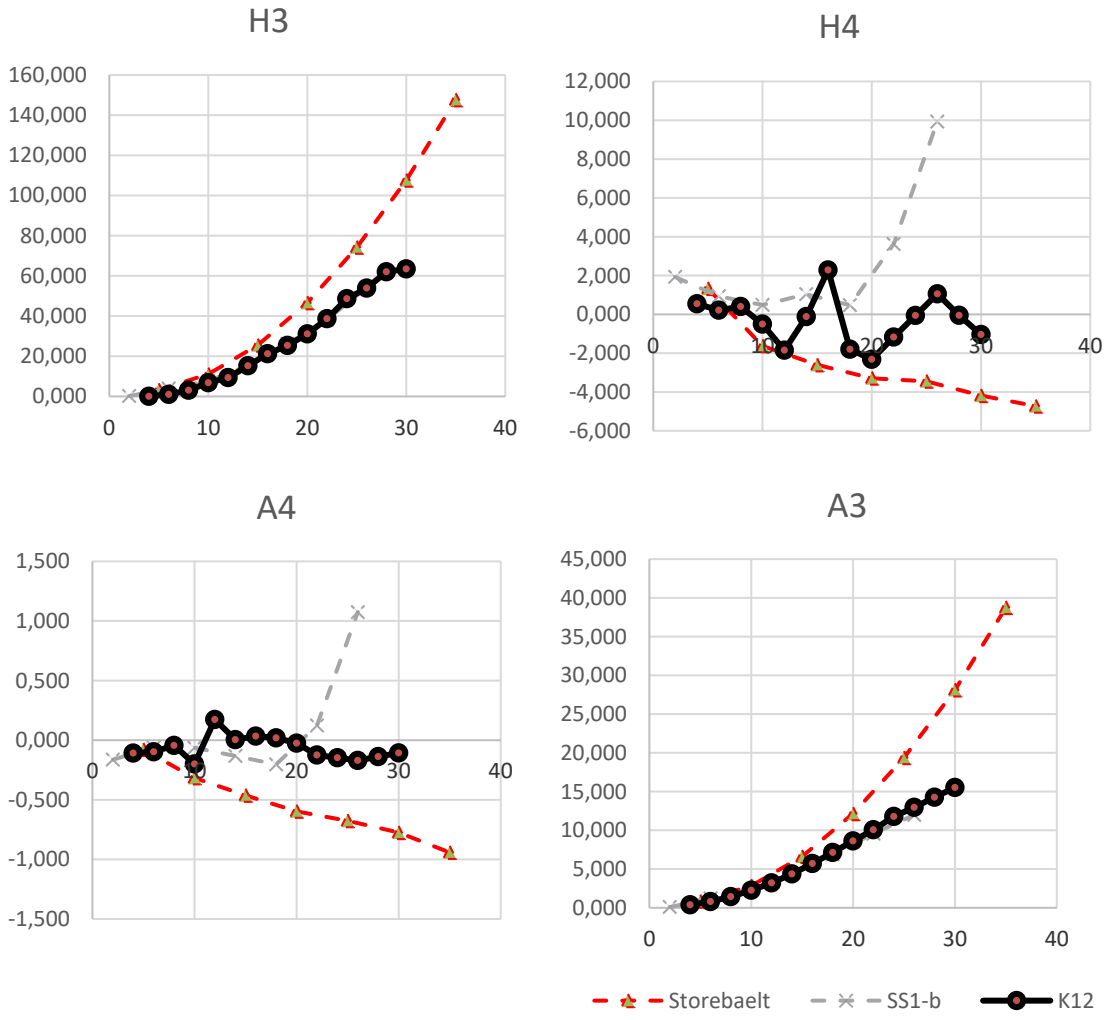

Figure 8 Aeroelastic stiffness flutter derivatives for; Storebaelt wind tunnel experiment, previous design cross section SS1 and latest design cross section K12

5 Conclusion

The aerodynamic and aeroelastic forces were successfully extracted for the cross section K12. The values have been compared to the reference examples, showing similar values, thus confirming the reliability of results. The presented results offer good starting design values, however they should be future validated by experiments or more sophisticated numerical models.